

RESIDUAL WELDING STRESS IN MEDIUM AND  
HIGHLY RESTRAINED WELDMENTS

by

William A. Komlos

A thesis submitted to the faculty of  
The University of Utah  
in partial fulfillment of the requirements for the degree of

Master of Science

Department of Civil and Environmental Engineering

The University of Utah

May 2009

Copyright © William A. Komlos 2009

All Rights Reserved

THE UNIVERSITY OF UTAH GRADUATE SCHOOL

**SUPERVISORY COMMITTEE APPROVAL**

of a thesis submitted by

William Arthur Komlos

This thesis has been read by each member of the following supervisory committee and by majority vote has been found to be satisfactory.

11/2/07

  
Chair: Lawrence D. Reaveley

11/2/07

  
Chris Pantelides

2 NOV 2007




THE UNIVERSITY OF UTAH GRADUATE SCHOOL

**FINAL READING APPROVAL**

To the Graduate Council of the University of Utah:

I have read the thesis of William Arthur Komlos in its final form and have found that (1) its format, citations, and bibliographic style are consistent and acceptable; (2) its illustrative materials including figures, tables, and charts are in place; and (3) the final manuscript is satisfactory to the supervisory committee and is ready for submission to The Graduate School.


  
\_\_\_\_\_  
Date

  
Lawrence D. Reaveley  
Chair: Supervisory Committee

Approved for the Major Department

  
Paul J. Tikalsky  
Chair/Dean

Approved for the Graduate Council

  
\_\_\_\_\_  
David S. Chapman  
Dean of The Graduate School

## ABSTRACT

Restrained welded structures hold significant residual strains that preload the structural system, robbing the structural capacity expected by design. Shrinking weld metal and thermal joint displacement combine to create residual stress in the welded connections. Residual welding stress combines with other processing stresses remaining in the individual members or preassembled components. Whether the combinations of all residual stresses result in a compressive or tensile applied force depends upon the geometry of the structural members and the direction of applied internal loads. Regardless of magnitude, residual stresses become part of the forces applied during service. Safety factors incorporated into structural design, typically 1.65, are thought to address the impact of residual stress.

Residual welding stresses in heavy weldments are tensile in all three planes. The reaction of the massive joint against displacement increases the magnitude of resultant tension. Tension along all three axes, triaxiality, promotes a state of plane-strain stress in the weldment. Steels at plane-strain stress, where metal cannot stretch or yield, can fail at loads below those anticipated by design. Triaxial tension reduces the ductility of structural systems.

The heat of the welding arc drives residual welding stress. The hottest spot is located immediately beneath the arc and temperatures decrease to ambient temperatures at some distance from the weld. Cooling rates are very fast under the arc but slow in the regions surrounding the arc as the thermal gradient declines. The welding arc furnishes

the energy that causes the weld metal to shrink and the surrounding base metal to expand at the same time.

Welding Codes identify three joint restraint conditions: low, medium, and high. Production costs increase dramatically as joint restraint increases. No welding Code, however, offers defining attributes for restraint conditions. This thesis evaluates residual strain in a moment-frame while welding the beam-to-column connections. Data obtained during three experiment series describe the welding effects on pinned and fixed joint configurations. Experimental data will characterize joint restraint in medium and highly restrained connections. A structural analysis of an actual large-span truss shows the effect of numerous small displacements at each truss connection node.

## TABLE OF CONTENTS

ABSTRACT.....	iv
LIST OF TABLES.....	viii
LIST OF FIGURES.....	ix
SYMBOLS AND ABBREVIATIONS.....	xi
ACKNOWLEDGMENTS.....	xii
INTRODUCTION.....	1
Chapters	
1. LITERATURE SEARCH.....	4
1.1. The Northridge Earthquake Paradigm Shift.....	4
1.2. Common Computer Models.....	6
1.3. Complex Computer Models.....	9
1.4. Stress and Displacement.....	13
1.5. Joint Restraint.....	24
2. EXPERIMENTAL PROGRAM.....	34
2.1. The Structural Bounds of the Beam-to-Column Welded Connection.....	34
2.2. The Test Assembly.....	45
2.3. The Beam-to-Column Weld Connection.....	50
2.4. Location and Selection of Gauges.....	54
2.5. Gauge Correction.....	56
2.6. Gauges in the Welding Environment.....	57
2.7. Experiment Methodology.....	58
3. EXPERIMENTAL RESULTS AND DATA ANALYSIS.....	62
3.1. General Considerations in the Data Analysis.....	62
3.2. Analyzing Strain Gradients.....	71
3.3. Analysis of the LVDT Data for Joints Under Medium Restraint.....	75
3.4. Analysis of the LVDT Data for Highly Restrained Joints.....	78
3.5. Calculating the Resultant Stress.....	82

3.6.	Joint Restraint and the AWS Displacement Equations.....	88
3.7.	Evaluation of a Long-Span Truss .....	90
4.	CONCLUSIONS.....	95
4.1.	Characterization of Medium and High Joint Restraint .....	95
4.2.	Welding Displacement and Medium Joint Restraint .....	97
4.3.	Weld Tempering .....	98
4.4.	Fabrication Sequences .....	98
5.	RECOMMENDATIONS FOR FURTHER STUDY.....	100
	REFERENCES .....	103



## LIST OF TABLES

<u>Table</u>	<u>Page</u>
1. Mechanical Properties of Materials .....	50
2. WT Beam Schedule and Joint Restraint .....	60
3. Resultant Residual Strain.....	72
4. Resultant Residual Stress.....	72
5. Displacement Data Detail ~ Medium Restraint, Far Column.....	78
6. Displacement Data Detail ~ Medium Restraint, Adjacent Column.....	78
7. Displacement Data Detail - High Restraint, Adjacent Column .....	80
8. Displacement Data Detail ~ High Restraint, Far Column .....	80
9. Change in Residual Stress – Displacement Gauges.....	86
10. Change in Residual Stress - Strain Gauges.....	86
11. AWS Predicted Displacement Versus Actual Displacement.....	89
12. Method of Virtual Work - Displacement at Point H.....	94

## LIST OF FIGURES

<u>Figure</u>	<u>Page</u>
1. Mohr's Circle (a) and (b).....	16
2. Moduli of Elasticity .....	19
3. Thermal Gradient at a Beam-to-Column Connection.....	21
4. Thermal Displacement .....	23
5. Free-Body Diagrams of Welded Rigidity .....	26
6. Simple Beam - Concentrated Load .....	39
7. Location of the Applied Load .....	40
8. Elevation View of a Long Span Truss .....	44
9. Test Frame and Gauge Locations .....	46
10. Rolling Directions .....	48
11. Welding Procedure.....	54
12. Typical Weld Joint Preparation .....	61
13. Graph - Strain Versus Time, WT-1, Joints 1 & 2 .....	63
14. Graph - Strain Versus Time, WT-2, Joints 3 & 4-1 .....	64
15. Graph - Strain Versus Time, WT-3, Joints 3 & 4-1 .....	65
16. Graph - Strain Versus Time, WT-3, Joint 4-2 .....	66
17. Graph - Displacement Versus Time, WT-1, Joints 1 & 2.....	67
18. Graph - Displacement Versus Time, WT-2, Joint 3 & 4-1 .....	68

19. Graph - Displacement Versus Time, WT-3, Joints 3 & 4-1 .....	69
20. Graph - Displacement Versus Time, WT-3, Joint 4-1 Removal and Joint 4-2.....	70
21. Displacement Versus Time, WT-2, Joint 4-1 Removal.....	83
22. Graph - Strain Versus Time, WT-2, Joint 4-1, Removal.....	84
23. Graph - Strain Versus Time, WT-3, Joint 4-1, Removal.....	85
24. Analysis of a Truss at Point H .....	91
25. Truss Connection Free-Body Diagrams.....	92

## SYMBOLS AND ABBREVIATIONS

A = area

$A_{\text{Beam}}$  = Area of beam,  $\text{cm}^2$  ( $\text{in}^2$ )

$A_{\text{col}}$  = Area of column,  $\text{cm}^2$  ( $\text{in}^2$ )

$A_w$  = cross sectional area of weld,  $\text{cm}^2$  ( $\text{in}^2$ )

$C_3$  = 12 or 305 when L and t are in inches or millimeters, respectively

E = Young's modulus, = 200 GPa (29,000 ksi),  $\sigma/\epsilon$

I = Second moment of inertia

J = Joules

L = overall length

$L_{\text{Beam}}$  = Length of member

$L_{\text{col}}$  = Length of column

$L_{\text{WZ}}$  = Length of weld zone

$L_1$  = Length of material at ambient temperature

$L_2$  = Length of material between ambient temperature and  $649^\circ\text{C}$  ( $1200^\circ\text{F}$ )

$L_3$  = Length of material above  $649^\circ\text{C}$  ( $1200^\circ\text{F}$ )

$\Delta L$  = change in length, displacement

P = Load

$\Delta T$  = Change in temperature from ambient

V = travel speed (inches per minute or millimeters per minute)

a = Distance<sub>1</sub> along column axis, in

b = Distance<sub>2</sub> along column axis, in

d = root opening, in.

n = a virtual load

t = thickness of plates, in.

u = a virtual displacement

$\epsilon$  = strain

$\delta$  = Actual displacement

$\sigma$  = stress

$\sigma_{\text{max}}$  = Maximum stress measured under load

$\sigma_{\text{min}}$  = Minimum stress measured under load

$\sigma_{\text{uts}}$  = Ultimate tensile stress

$\tau$  = shear stress

$\tau_{\text{cr}}$  = critical shear stress needed to cause displacement

$\alpha$  = Coefficient of thermal expansion for mild steel,  $^\circ\text{F}^{-1} = (6.1 + 0.0019t) \times 10^{-6} \text{ }^\circ\text{F}^{-1}$

$\Delta_{\text{trans}}$  = transverse shrinkage, in.

## ACKNOWLEDGMENTS

This thesis is dedicated to my wife, Carol, my daughter, Robin, and my mother, Joann Meigs. Their support and understanding of the effort needed to accomplish this work was unflagging and greatly appreciated.

The author wishes to thank SME Steel Contractors, The Mark Steel Corporation, Blue Star Steel LLC, Praxair Corporation, A & F Welding, MSI Testing Incorporated, and Ironworkers Local Union 27 for providing the materials, services, and labor needed to perform this self-funded thesis. The experiments would never have taken place without the support of these generous benefactors. They never asked why; they only asked how much.

The author also wishes to thank the University of Utah Structures Lab Manager, Mark Bryant, who oversaw the installations performed by two student technicians, Shannon Hanson and Tyler Ross. Special thanks to Todd Anderson, Certified Welder, CWI, and CWE for the Ironworker Apprenticeship Program who performed the welding on this portion of the experiments. These people lived with this project and saw its ups and downs. Their confidence helped push it forward.

## INTRODUCTION

The author conducted experiments at the Structures Laboratory of the University of Utah to characterize the residual welding stresses resulting from joint restraint. Joint restraint is assumed in all welds, but not readily identified in construction codes or engineering literature. A weld joint between two bars, with both ends free, offers little restraint to the shrinking weld. The closing weld of a moment-resisting frame, on the other hand, is highly restrained and can resist displacement in three axes. As joint restraint increases, the stress in the structure created by welding also increases. This welding stress remains in the structure until relieved by material yielding or supplementary stress-relieving operations. Residual welding stress robs connections of the strength expected by the structural design.

Construction codes developed by the American Institute of Steel Construction (AISC) and the American Welding Society (AWS) categorize three degrees of restraint: low, medium, and high. They leave the engineer, however, with the responsibility for defining the limits and bounds of these categories. AWS recognizes that it is impossible to define restraint more explicitly at this time. They have made a clear call to Industry for a concerted surveillance program that will eventually classify the details and situations describing these restraint levels. In response to Industry's need for quantitative data, this thesis explores the structural bounds of medium and highly restrained joints.

Full-scale moment-resisting frames were welded together, cut apart, and welded again over three test series. To construct the frame, two welded connections joined a

horizontal beam between two upright columns: one pinned connection and one fixed. The joint geometry followed common beam-to-column drafting details and was almost identical at each connection. The joints were filled following the same welding parameters. The welding stress induced into the structural frame while welding the pinned connections was lower than the stress in the fixed connections. The beam moves unrestrained longitudinally while the first end is welded to a column. The pinned connection at equilibrium retained areas of compression. The beam is highly restrained and the first end completely fixed in the structure while welding the final closing joint. All of the fixed connections were under higher tensile stress after welding. No compressive stress remained. The relative degree of joint restraint completely changed the stress gradient in the welded frame.

This thesis also examines the effects of welding on a 145 Mg (160-ton) truss. Today's structural designers draw upon larger and larger structural sections to support longer spans and larger loads. Recently, designers installed large trusses to support water-stages and hydraulics used in a popular aqua-theater. The jumbo structural sections used to fabricate the truss were identical to the sections employed in the present experiments. The 57 mm (2-1/4 in.) thick connecting joints are highly restrained in all three planes. The joint configurations of the actual truss are similar to the present experiments and the data obtained by testing can be applied to this existing structure. The author employed the method of virtual work to analyze the displacement caused by shrinking welds and thermal gradients in the truss members. The displacement obtained from this analysis was significant. When the results were compared to the limits imposed by AISC and AWS, free displacement would make the trusses unsuitable for use. Restraining the weldments

with fixtures and erection aids, while maintaining dimensional integrity, only serves to increase the residual welding stress in the structure. Contractors of all large-scale structures face this dilemma. This thesis offers recommendations to reduce residual stresses in joints under high restraint. --



## 1. LITERATURE SEARCH

### 1.1. The Northridge Earthquake Paradigm Shift

The structural steel failures observed after the 1994 Northridge earthquake in California identified the need for more research in highly restrained connections. Traditional structural designs focused upon structures strong and stiff enough to resist bending and twisting expected during seismic and ballistic events. When typical connections used in these designs were checked after the earthquake, investigators found cracked welds, beams, and columns. Investigators discovered that the many structural members failed by fracture during the earthquake at very low levels of plastic demand with little or no yielding (FEMA 2000).

In 2000, the SAC Joint Venture investigated the effects of seismic events on structural steel designs and proposed modifications to improve seismic performance. The SAC Joint Venture combined the efforts of the Structural Engineers Association of California, the Applied Technology Council, and the California Universities for Research in Earthquake Engineering. Their document established design improvements that were identified by the tests and models funded by the Federal Emergency Management Agency. These improvements have resulted in ductile designs more resistant to fracture. These new designs include such ideas as the reduced beam section connection to force plastic deformation into the connecting beam, proprietary designs such as the *SidePlate*<sup>™</sup> connection, and the buckling restrained brace. The SAC Joint Venture also drove improvements in the governing welding Code. The American Welding Society released

AWS D1.8, Structural Welding Code – Seismic Supplement. This supplement mandates very strict heat input levels for welding, previously not considered for common structural steels.

Immediately after this paradigm-changing earthquake, two families of connections were developed to improve design performance. They can be categorized as the “stiff” group and the “ductile” group. Some designers revised their connections to stiffen the joints to resist seismic and ballistic forces. In some designs, secondary plates are added on the outside surfaces of the top and bottom flanges of the connecting beams. Other designs use complex plate configurations attached to the columns to force beams to plastify away from the column face. These secondary plates not only stiffen the connections, but also add extra labor to fabricate and attach them. Other designers removed material at key locations designing beams that plastify at locally weaker regions built into the load-resisting system. Highly detailed weld access holes, slots removing material between beam webs and flanges, and cuts in beam flanges to reduce section width are incorporated into today’s design, again, to force a plastic hinge away from the column face. Except for the Buckling Restrained Brace, these connection families depend upon welds to fabricate moment-resisting frames. Neither of these connection families do anything to reduce the residual effects of welding.

The weld zone of the moment weld had not been well described or investigated before the Northridge earthquake. Engineers have long understood that simple beam theory did not describe the discontinuity at the weld zone. The design load paths make a sharp change in direction, as grain orientation of structural members’ changes; and even the material mechanical properties are significantly different in this tiny portion of the

overall structure. Common thought believed that as long as the weld metal strength exceeds the base metal strength, the connection would be superior to the original base material and perform as designed. The SAC Joint Venture investigated the performance of the connections. Later investigators used computer models to analyze the weld zone at the connection.

## 1.2. Common Computer Models

In 2000, Zhang and Dong modeled the residual stresses in welded moment frames typical of the Northridge investigations. As lead research scientists for the Battelle Memorial Institute, this team has been responsible for numerous articles on residual welding stress. Their research is typical of detailed finite-element computer analysis and incorporates data from physical experiments performed by others to characterize the effects of residual welding stress on structural performance. Several assumptions introduced in their welding model treat residual welding stress as a stress preloading the connection area before service. Their model did not quantify the global effects of the structure on the connection or the intermediate effects of repeated heating and cooling while welding and preheating. Their model characterized the direct effects of a welded joint in the regional connection of a structural frame (Zhang and Dong 2000).

The model initially lumps the virtual weld into one pass in 25 mm (1-in) plate. They refine their model to include nine passes in 35 mm (1-1/2-in) flanges incorporating experimental data taken in 1985. This welding model may be accurate for relatively thin sections. It cannot evaluate, however, any locking effects the initial five or six weld passes have on the joint. The present experiments, with 30 or more weld passes in the flange-to-column joint, show the solidified initial passes act to resist joint displacement.

These initial passes rapidly increase the residual stresses observed during welding.

The weld configuration and the thickness range the computer model by Zhang and Dong (2000) cannot evaluate the effects of triaxial stress in structural steel connections. The weld model applies welds to the beam flanges only and no compensating weld is applied to the web. The beam is not fully fixed to the column in the virtual configuration. The present experiments show that the column flange bends around the flange weld while welding progresses. The model incorporates relatively thin sections. The model is derived from SAC tests and many of these tests were performed on various configurations of the standard common 13 mm (.505) tensile test. A typical uniaxial tensile test exhibits considerable necking or reduction of area before ultimate failure. Even when prepared to promote fracture, some ductility in the coupon remains. Necking is restricted only when test coupons are not machined to provide a reduced section or a maximum thickness is exceeded. AISC design and AWS welding codes expect that large steel sections, 35 mm (1-1/2-in) thick or greater, resist displacement and promote fracture. This size is three times larger than the common tensile test coupon.

The yield strength of the beam used in the model is assumed to conform to a range of yield strength expected for true, low-strength ASTM A36 material. No actual mechanical test data were used to formulate the model. Actually, producing mills have dual-certified their wide-flange sections to comply with both ASTM A36 and the stronger ASTM A572 gr 50 since before the Northridge earthquake. The author's experience indicates true A36 wide-flange sections have not been commercially available for more than 25 years, as the wide-flanges were made stronger to facilitate lighter, economical designs. The lower strength beams in the Zhang and Dong (2000) model effectively

dampen crack energy release rates and lower the stress intensity at the crack tip. In this model, the energy release rate stops increasing after the applied load reaches the initial yield strength of the beam material. It is more likely, however, that the beam mechanical properties are closer to the column properties than the model assumes. Zhang and Dong (2000) recognize that stresses intensify crack growth in higher strength structural material. The crack driving force will suddenly increase at full yield if the yield strengths of the base metals and weld filler metal are more homogenous. Higher stress intensity at the crack tip will promote catastrophic fracture of the joint.

The virtual filler metal, E70T-4, is much stronger than the base material, it is not fracture-rated, and is not permitted for use in today's seismic or fracture-critical applications. The slag system cleaning and protecting the resulting weld incorporates an aluminum-based deoxidizing system. This shielding system develops a weld that is strong and hard, but prone to cracking under dynamic loading. The mechanical data obtained in 1985 identify the weld metal as the strongest material in the weldment and compare with the data obtained during tests performed by the author in 2001. Zhang and Dong (2000) are aware of this metallurgical discontinuity but do not investigate it in any detail in their model. The Zhang and Dong (2000) model assumes mechanical welding flaws will cause the weld metal to fail before the base metal. This may not be the case if tough weld filler metal is used in the joint.

Zhang and Dong (2000) describe regions in the weld with the greatest tensile residual stress. Their model develops tensile residual stress as high as 100 MPa (29 ksi) in the top third of the flange-to-column weld. This compares well with the approximately 138 MPa (20 ksi) measured 305 mm (12-in) away from the weld joint during the present

experiments. Their model develops tensile residual stresses as high as 1000 MPa (145 ksi) at the weld root. They never discuss how these levels can occur in common structural steels without fracture. Only a highly restrained joint with increased material properties would tolerate these very high local stresses. Their model illustrates why mechanical welding flaws at the weld root reduce the structural performance of the weld joint. High tensile residual stress significantly elevates the fracture driving force on small discontinuities in this model. Zhang and Dong (2000) predict fracture will occur well before the beam yields when tensile residual stress is present. This agrees with what has been observed in a highly restrained joint.

### 1.3. Complex Computer Models

In contrast to the Zhang and Dong (2000) model investigating residual stresses in weldments, others have developed models to describe the high levels of stress triaxiality that results when welding moment frame connections. The Schafer et al. (2000) finite-element model assumes the same base material configuration at the joint as the Zhang and Dong model (2000): an A36 beam, A572 gr 50 column, and E70T-4 filler metal. Schafer et al. (2000) compare their results with SAC full-scale tests that reported actual material mechanical properties. In the SAC experiments, the yield strength of the beam was greater than the column: 418 MPa (60.6 ksi) and 333 MPa (48.3 ksi), respectively. The SAC beam is actually stronger than the columns and beams used in the present experiments. The column yield strength is below the minimum requirements of A572 gr 50. These material discrepancies are not addressed by Schafer et al. (2000). These investigators also neglect the weld filler metal's lack of fracture toughness. They rely upon filler metal data published by Blodgett in 1976.

The research by Schafer et al. (2000) is unique in its understanding of material strength and joint restraint. Their model clearly defines triaxiality for the reader as the ratio of the maximum principal stress at a point to the Von Mises stress. Under this definition, if triaxiality for standard uniaxial tensile test is 1, triaxiality under multiaxial states of stress can be greater than 1. The Von Mises stress corresponds to the standard uniaxial tensile stress shown on material test reports. But the maximum stress at the connection can be greater than the Von Mises stress and greater than the ultimate design tensile strength. This anomaly can be caused by changes in temperature, rates of loading, and joint constraint due to thickness, geometry, differences in material strengths at the weld, and combinations of these causes. It is the combination of causes changing material properties for a particular condition that make any analysis of plane-strain stress so complex and difficult to evaluate.

The Schafer et al. (2000) model analyzes the end condition of the beam-to-column connection. This region is not generally considered in steel design and the researchers found it does not conform to conventional beam theory. Their model locates the maximum shear near the beam flanges and the minimum shear near the centroid of the beam. Their finding contradicts conventional beam theory. At fracture, they discover the top of the beam flange is essentially unloaded over a significant portion of its width, also contradicting beam theory. Beam theory presumes that the beam bottom flange is in uniform tension in the plastic case or having a small stress gradient in the elastic case. The Schafer et al. (2000) model of the pre-Northridge connection locates the maximum stress and triaxiality demands in the beam bottom flange at the column face below the web, not at the backup bar as described in research literature or along the flange width.

These researchers explain that as the connection goes through increasing rotation during loading, more material volume undergoes load demand while the maximum stress increases slightly. As the volume of material under load increases, the connection has a higher chance of fracture. Their model shows that the weld metal immediately above the backup bar plastifies at greatly elevated stresses because of the high triaxiality. The model indicates 50% of the material volume is at a stress greater than 550 MPa (80 ksi), much higher than the properties of the individual materials by themselves.

Schafer et al. (2000) recognize most models used in finite-element analysis are not sufficiently complex to incorporate accurately the impact of triaxiality on a structural connection. Because of the several variable factors that influence the magnitude of the triaxial stress state at the joint, one-parameter fracture mechanics models ( $K_c$ ,  $J$ , and CTOD) are insufficient for accurate characterization. These models are especially limited for ductile metals that undergo large-scale plasticity and where welding flaws do not influence the failure mode. These researchers recommend using 3D, nonlinear finite-element analysis to evaluate welded steel moment frame connections. Fracture of these connections may be governed by triaxiality even when high toughness parent and weld metals are used in design.

Though numerous computer models have been developed since the 1994 Northridge earthquake, today's literature provides little guidance for the engineer to quantify or characterize residual welding stresses. The AISC (2005) in their section on Avoiding Brittle Fracture offers only this support to the designer of heavy steel weldments:



Generally, a brittle fracture can occur when there is a sufficiently adverse combination of tensile stress, temperature, strain rate, and geometrical discontinuity (notch). The exact combination of these conditions and other factors that will cause brittle fracture cannot be readily calculated. Consequently, the best guide in selecting steel material that is appropriate for a given application is experience. (AISC 2005, p. 2-33)

Unfortunately, most structural engineers have little experience in welding, joint restraint, and the behavior of metals under the heat of the electric welding arc. The existing literature has not quantified the magnitude of the stress for them or described the restraint conditions that compound stress. The author needed better answers to consider the effects of restraint and heat on thick, heavy structures. A program of experiments was developed to measure over time the warps and twists that accompany the welding of structurally restrained joints. Experimental data observing the structural conditions contributing to residual stress would establish stress magnitudes and sequences needed to distinguish between different levels of joint restraint. Experimental data observing the physical displacement of the weld joint, the welded member, and the structural frame during welding would demonstrate the trade-off between freedom of restraint and the resultant residual stress.

The interplay between steel and heat is complex, however. Material strength changes when heated and temperature gradients displace the heated members with some effect on residual welding stress. To identify the physical structural conditions associated with residual welding stress, the author reviewed the fundamental metallurgical conditions needed to achieve ductile performance in welded connections. Stress shedding by weld temper beads and localized material displacement at preheat and interpass temperatures need to be addressed in any discussion of heavy welds. Engineers need some ability to predict welding displacement to develop robust welding plans. These

experiments apply these fundamental conditions at the level of the individual weld bead within the joint to illustrate the impact of welding on a large-scale structure.

## 1.4. Stress and Displacement

### 1.4.1. Hydrostatic and Deviatoric Displacement

Metals change shape when loads are placed upon them or when their temperatures change. Changes in temperature force metals to expand or contract hydrostatically in all three axes. Volumes change as temperature changes, but no permanent deformation takes place. Deviatoric displacement stretches or compresses metals from their original location. Deviatoric displacement enables metals to shed the load effects by stretching and necking. Elastically, metal stretches in one or two axes and thins in the other axis. When sufficient load is applied, metal will displace permanently in the loaded shape. Any activity that restrains either hydrostatic or deviatoric displacements induces reaction stresses in the metal and robs the metal of its ductility.

Applied loads change the shape of metal deviatorically in compliance with the forces that result under load. Dividing the load applied to a member by the member's area gives the stress applied to the member. Displacement by a load creates reaction stresses in the member, of opposite sign and normal to the direction of loading. These stresses are the result of the "Poisson effect" which observes transverse strain is a constant fraction of the strain in the longitudinal direction.

Metals slide along internal slip-planes under load. Each metal molecule slides along naturally evolving crystalline slip-planes in the grain structure. The slip-planes intersect one another within very strict crystalline structures that correspond to the chemical composition of the metal or alloy. Steel needs a minimum level of shear stress,

$\tau_{cr}$ , to stretch or deform deviatorically and maintain ductility. Shear stresses naturally develop as service loads are applied along the principal axes of the steel crystals. Only shear stresses,  $\tau$ , create deviatoric displacement (Dieter 1986). The shear stress through an element available for displacement under uniaxial load is simply calculated from Equation 1.

$$\tau = \frac{\sigma_{\max} - \sigma_{\min}}{2} \quad (1)$$

where  $\sigma_{\max}$  = the maximum most positive stress thru an element; and  
 $\sigma_{\min}$  = the minimum stress.

Shear stress and the Poisson effect are readily observed during tensile testing. An increasing axial load forces the test specimen to stretch. Test specimens are typically machined down in their centers to reduce the local area and promote failure. Necking from the Poisson effect is observed as the reduced section draws down thinner and thinner until the specimen abruptly snaps at the ultimate tensile load,  $\sigma_{\text{uts}}$ .

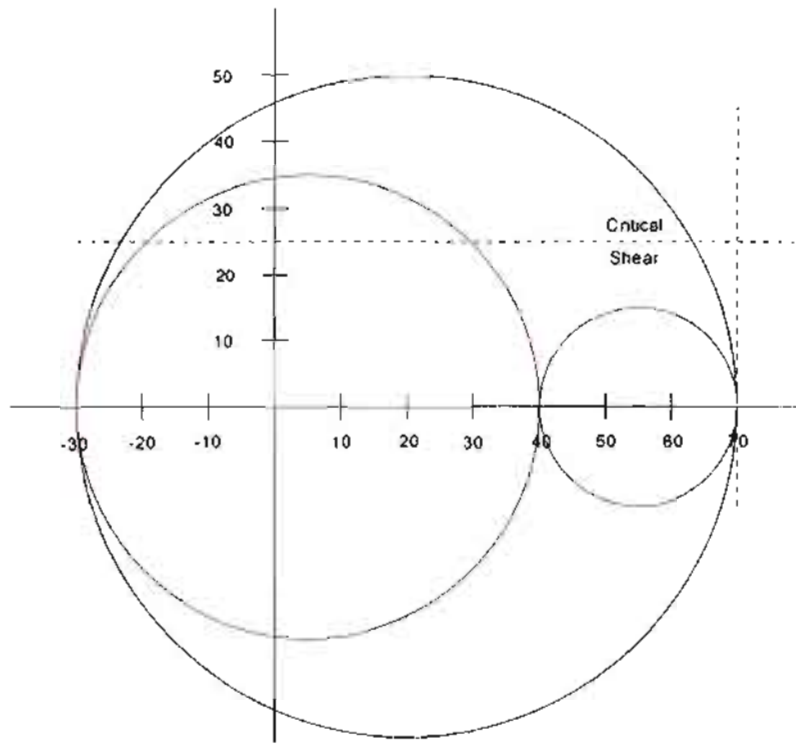
Steel can store significant amounts of energy, displacing elastically or by permanent deformation. Shear stresses in a ductile connection freely build to the critical level. Deviatoric displacement proceeds elastically while the available shear stress remains above the critical shear stress. In a ductile steel member, stress can increase until the yield strength is exceeded. This point is where steel stops storing stress elastically and permanently distorts plastically. Stress in the member does not significantly increase during plastic deformation, but the member stretches dramatically. Plastic deformation proceeds until the ultimate tensile stress is reached and the member breaks apart. A

ductile failure in steel cleaves along a 45-degree plane from the load axis of the specimen. The fracture line follows the slip-planes upon which the shear stress worked.

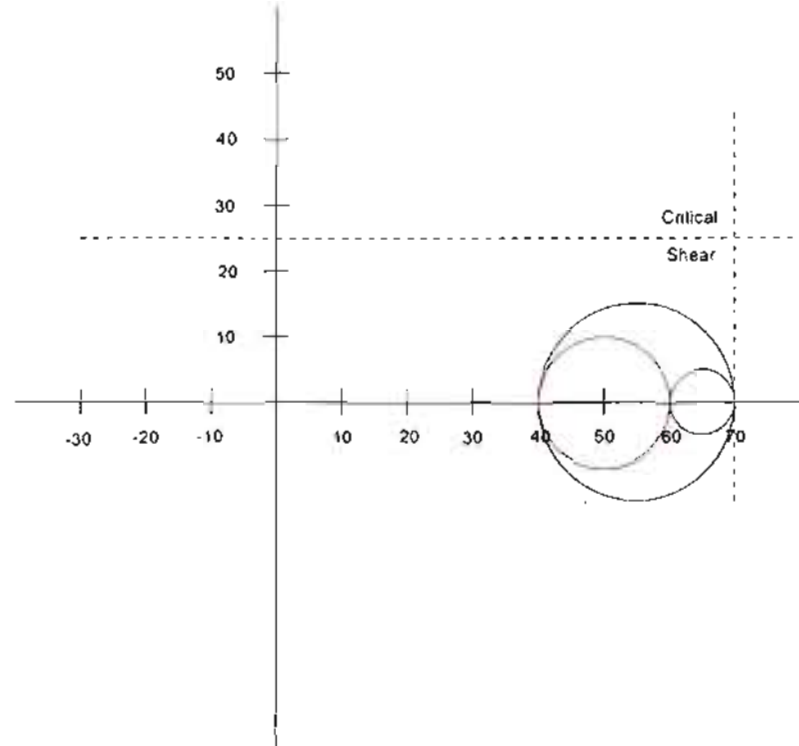
When displacement in a member or a connection is restrained in all three planes and no displacement can occur, that member is in a plane-strain stress state. A shrinking weld pulls against the adjoining base metal in all three planes and, triaxially, the principal stresses in the connection are tensile. Complex connection configurations such as the T-K-Y node in a space truss or the moment weld in a special moment frame restrict deviatoric displacement along slip-planes and trap hydrostatic thermal displacement in the cooling welds. The state of plane-strain stress restricting displacement prevents the deviatoric stresses from every reaching the critical shear stress. Mohr's Circle illustrates why triaxial tensile stresses reduce the shear stress available for deviatoric displacement.

#### 1.4.2. Mohr's Circle

Figure 1 graphically illustrates the effect of tension in all three planes on available shear stress. As long as  $\sigma_{\min}$ , the minimum stress in the system, is zero or compressive, the shear stress available for deviatoric displacement is maximized. But when the minimum principal stress is also tensile, the shear stress available for deviatoric displacement is reduced. Thin material cannot resist the Poisson effect through its thickness so at least one principal axis adds zero stress to the system and maximum shear stress is always available. Thick material will hold a load and a plane-strain state develops in the steel crystals. Little or no shear stress is available to displace the metal. Any condition restricting necking reduces the potential ductility of the member. There is a potential that the restraint of a connection in plane-strain stress state will restrict the available shear stress and  $\tau_{cr}$  will not be reached.



(a)



(b)

Figure 1. Mohr's Circle (a) and (b)

Stress applied along the principal axes of steel crystals, the horizontal axis of Mohr's Circle, induces shear stress along the slip-planes, represented by the vertical axis. Figure 1(a) describes the stress interactions of a thin, unrestrained member. Each circle can represent the stress system and available shear stress along slip-planes in three dimensions. Two of the planes possess a cushion of compression. One plane does not. The compression cushion in two planes affords all planes shear stress in excess of  $\tau_{cr}$ . Even one plane in compression prevents triaxial stress from building in the member. Figure 1(b) describes a highly restrained member in triaxial stress. A member under triaxial stress is prone to failing in a brittle manner before it yields. All planes are in tension and the shear stress is not sufficient to exceed  $\tau_{cr}$ . The member has little ductility and yielding is restrained. Any activity that increases the tension residing in a member or a connection ultimately reduces its ductility.

#### 1.4.3. Young's Modulus, the Modulus of Elasticity

Young's Modulus ( $E$ ), the modulus of elasticity, describes the interaction of strain,  $\epsilon$ , with the stress applied through a member. Within its elastic range, steel displaces in direct proportion with any applied stress. When displacement is restricted or restrained, the stress is not shed but stored elastically in the final structural connection.

Steel displaces proportionally to changing temperatures. Thermal displacement from the heat of the welding arc becomes increasingly restrained during welding. Stress is stored in the connections. The combination of welding and thermal displacement is called residual welding stress. Equation 2 expresses stress-shedding displacement,  $\Delta L$ , as a function of Young's Modulus ( $E$ ) and external load. Length, area, and modulus of elasticity are all physical properties of the structural member (Dieter 1986).

$$E_{steel} = \frac{\sigma}{\varepsilon} = \frac{\frac{P}{A}}{\frac{\Delta L}{L}}; \Delta L = \frac{PL}{AE} = \frac{\sigma L}{E} \quad (2)$$

where A = area; E = Young's modulus of elasticity; L = overall length;

$\Delta L$  = change in length, displacement; P = load;  $\varepsilon$  = strain; and  $\sigma$  = stress.

The modulus of elasticity for steel changes with changes in temperature. The yield strength of steel,  $F_y$ , decreases as the temperature of steel increases. At the melting point of steel, 1482°C (2700°F), E has reduced to 0. Liquid steel cannot support any strain. Steel creeps and sags under its own weight at temperatures above 732°C (1350°F). As steel cools below this temperature, its yield strength increases, supporting loads once again. In actual practice, multipass welds cool below this range within minutes. In thick welds, some regions of the weld joint will be at preheat temperatures, whereas other regions will be heated above the upper critical temperature. Figure 2 illustrates steel's changing resistance to elastic deformation as temperatures change.

#### 1.4.4. Thermal Displacement

Metal expands when heated and shrinks as the temperature cools. Thermal effects go to zero when thin sections or unrestrained connections are welded. Thermal displacement calculations for steel welds should begin at approximately 732°C (1350°F) and cooler. This is the first temperature along the thermal gradient where steel can carry structural loads. Increasingly thick material or higher joint rigidity resists the displacement needed to completely mitigate the residual welding stress. Decreasing temperatures predict the hot weld metal will shrink. But base metals will locally expand

Moduli of Elasticity, E, For Given Temperatures  
For C-Mn-V Steels

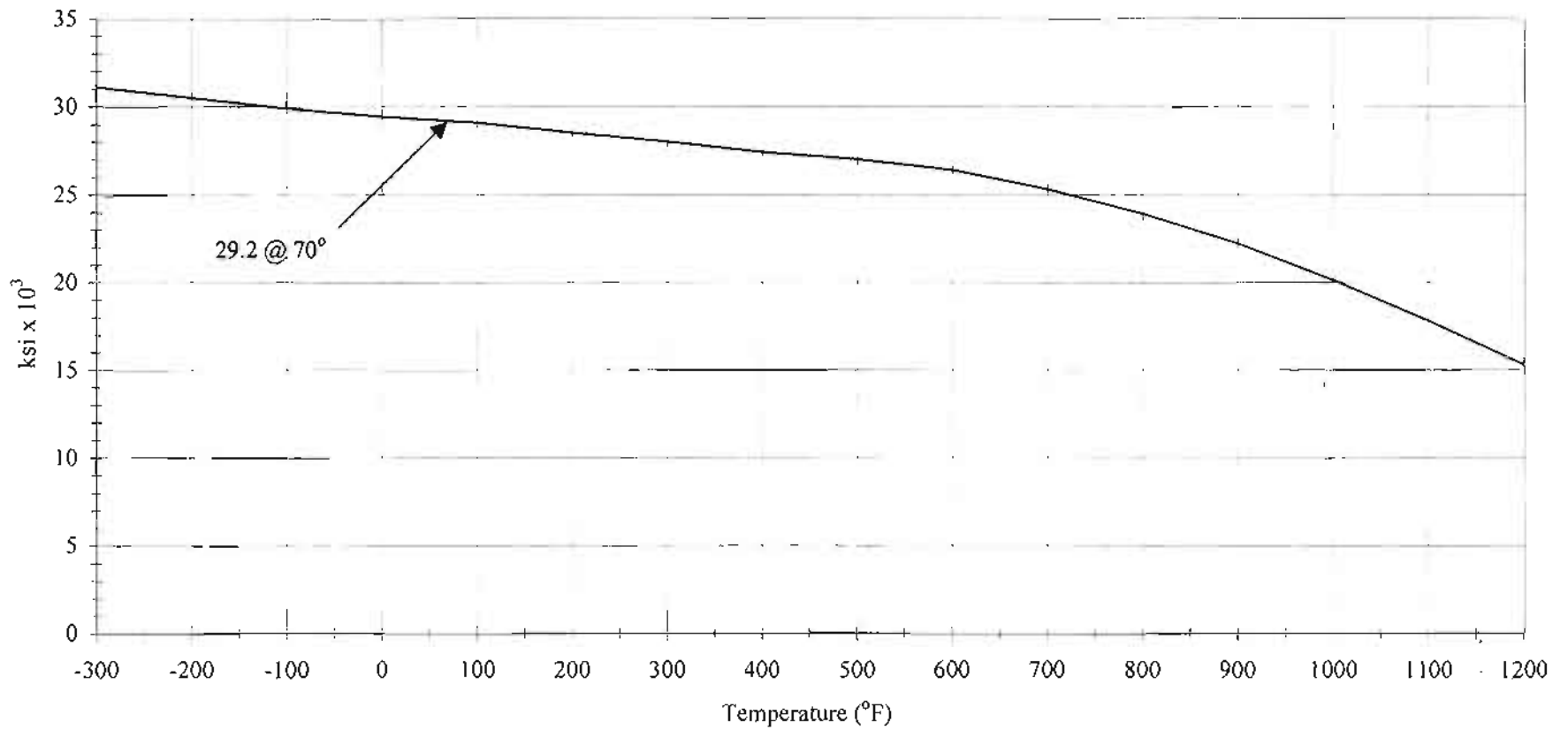


Figure 2. Moduli of Elasticity



and shift with any increase in temperature. Analyzing what effect increasing temperature has on a structural frame is very complex.

The present experiments recognized three regions describing the thermal gradient from welding.  $L_3$  was arbitrarily set at 25 mm (1 in) from the center of the welding arc. It represents the length of steel at the highest arc welding temperatures of liquid steel, approximately  $1482^{\circ}\text{C}$  ( $2700^{\circ}\text{F}$ ), where  $E$  is zero. These temperatures drop within seconds and the solidifying weld quickly contracts.  $L_2$  represents the very hot region from  $649^{\circ}\text{C}$  ( $1200^{\circ}\text{F}$ ) to  $38^{\circ}\text{C}$  ( $100^{\circ}\text{F}$ ) that extends from the end of  $L_3$  to approximately 305 mm (12 in) beyond the welding arc. The length of this region changes over time depending upon the metal thickness, joint configuration, and welding preheat. The base metal expands under these less extreme temperatures in region  $L_2$ .  $L_1$  represents the length of low temperature where temperatures return to ambient conditions. Thermal displacement is negligible in the  $L_1$  region. Lengths  $L_3$ ,  $L_2$ , and  $L_1$  are derived from experimental temperature data, but other lengths could be substituted. Further work is needed to more accurately describe the temperature over time.

The center of a thermal gradient is the welding arc temporarily radiating heat through the connection. The heat of the welding arc and the ancillary preheating maintenance operations produce the driving force for shrinking the weld metal and expanding the base metal. The heat directly under the arc is the highest and the metal beneath it is liquid at maximum expansion. Base metal away from the connection acts as a heat sink to pull heat out of the weld. Figure 3 illustrates the temperature gradient in a connection during welding. As long as heat is applied from an external source, steel temperatures increase over time. Residual heat is stored in the steel and radiates into the

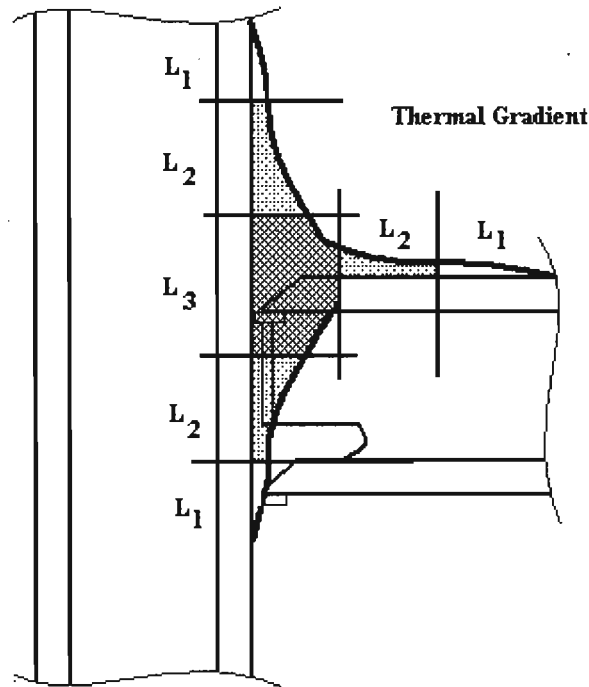


Figure 3. Thermal Gradient at a Beam-to-Column Connection

surrounding metal, increasing the length of Region  $L_2$ .

The components of residual welding stress are observed in the welding sequence. Tensile stresses created by the cooling weld metal pull against the colder, surrounding base metal. The temperature of the base metal immediately surrounding the weld varies, but is substantially hotter than ambient temperatures. This is the  $L_2$  region. This regional thermal expansion displaces members while welding continues. When the surrounding base metal finally returns to ambient temperature, the welded frame fixing the connection out-of-plane resists its return to the original length or location. All arc welding processes create similar welding stresses. The root opening and joint design determine the magnitude and distribution of residual stress (Masubuchi et al. 1987).

#### 1.4.5. Coefficient of Thermal Expansion

The coefficient of thermal expansion,  $\alpha$ , is a fundamental material property. It reflects the length changes per unit length of material for each degree change in temperature. Material charts developed for the National Boiler and Pressure Vessel Code report climbing thermal coefficients from  $11.5 - 15.1 \times 10^{-6} \text{ mm/mm/}^{\circ}\text{C}$  ( $6.4 - 8.4 \times 10^{-6} \text{ in/in/}^{\circ}\text{F}$ ) between  $21^{\circ}\text{C} - 704^{\circ}\text{C}$  ( $70^{\circ}\text{F} - 1300^{\circ}\text{F}$ ) (ASME 2001). AISC permits  $(11.0 + 0.0019 \times \text{the metal thickness}) \times 10^{-6} \text{ mm/mm/}^{\circ}\text{C}$  ( $(6.1 + 0.0019 \times \text{the metal thickness}) \times 10^{-6} \text{ in/in/}^{\circ}\text{F}$ ) as the coefficient when temperatures are above  $37.8^{\circ}\text{C}$  ( $100^{\circ}\text{F}$ ) (AISC 2005, p. 2-31). This thesis follows the AISC convention.

Equation 3 calculates the magnitude of thermal displacement in structural steels for changes in temperature. The equation is applicable to all steel member lengths and independent of volume. Applying the equation to the thermal gradient regions described in 1.4.4, Region  $L_3$  metal is fully expanded at liquid and almost liquid as the temperature nears  $1482^{\circ}\text{C}$  ( $2700^{\circ}\text{F}$ ). The superheated Region  $L_3$  is  $0.4 \text{ mm}$  ( $0.016 \text{ in}$ ) longer than the weld at ambient temperatures. Region  $L_2$  is  $0.13 \text{ mm}$  ( $0.005 \text{ in}$ ) longer because of the preheating before welding (Dieter, 1986). Tension in the cooling  $L_3$  region remains locked in the weld as residual tensile stress. The base metal around the weld, the  $L_2$  region, expands between  $2.4 \text{ mm}$  ( $.094 \text{ in}$ ) and  $0.4 \text{ mm}$  ( $0.016 \text{ in}$ ) because of the residual heat in the joint.

$$\Delta L = \alpha \Delta T L \quad (3)$$

where  $\Delta L$  = Change in length, displacement;  $L$  = Length of heated area at weld;  $\Delta T$  = Change in temperature; and  $\alpha$  = Coefficient of thermal expansion for mild steel.

Experimental data show that only the heated portions of the structural shapes expand while the portions at ambient temperatures maintain their original length. Region  $L_2$  displacement bends the column out-of-plane and bends the beam into a curving S-shape. Figure 4 illustrates the displacement that was observed in the experiments during welding. The thermal gradients are shown on the far side of the connection for clarity. The residual stress in the assembly changes as the cooling structural members attempt to straighten back to their original length at ambient temperatures. The balance of the structure at ambient  $L_1$  temperature resists thermal displacement in regions  $L_2$  and  $L_3$ . The  $L_1$  reaction force creates the thermal distortion in Region  $L_2$  and tension in Region  $L_3$ .

Equation 4 defines the cause of residual welding stress. Thermal displacement expressed in Equation 3 and displacements from imposed loads expressed in Equation 2 combine in  $\Delta L$  as the overall potential displacement available. Because structures store stress elastically, the actual displacement,  $\delta$ , is less than the overall potential

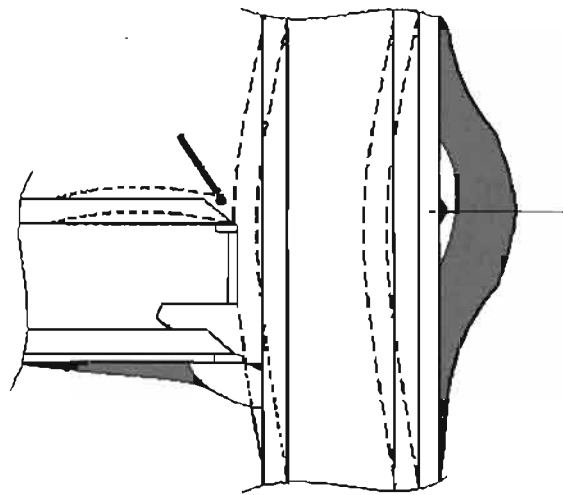


Figure 4. Thermal Displacement

displacement offered by the material constants. As the level of joint restraint increases, displacement expected from Young's Modulus or from the coefficient of thermal expansion is reduced. The difference between  $\delta$  and  $\Delta L$  reflects the residual stress remaining in the frame.

$$\begin{aligned} \text{When } \delta &= \Delta L, \sigma = 0; \\ \text{When } \delta &< \Delta L, \sigma = \text{Residual Stress} \end{aligned} \quad (4)$$

where  $\Delta L$  = Potential displacement;  $\delta$  = Actual displacement; and  $\sigma$  = stress.

The present data offer examples of potential displacement versus actual displacement. The experimental protocol required the beam to be cut apart. Joints always snapped open in this series of experiments when the last ligament was cut through. The welded frame in the thermally distorted condition described the actual displacement of the structural frame. The sudden gap at the cut beam visually expressed the difference between the actual displacement distorted by restraint and the potential displacement theoretically possible from the material equations. The release of restrained displacement previously welded into the moment frame released the residual welding stress in the structure.

## 1.5. Joint Restraint

### 1.5.1. Thermal Energy and Joint Restraint

Thermal displacement and residual processing stresses remain in the connection to strain the base metal from its original shape. Mechanically and thermally induced strain gradients remain that preload each connection of the resulting assemblies with stress. Stress is stored as elastic energy throughout the structure. Any resistance by the

structure to the created strain reacts to store stress. Stored, residual stresses are why structural wide-flange shapes “ring” when hit with a hammer. This stored energy waits to be released by yielding or cracking of the metal.

The structural reaction to residual welding stress increases as the weldment gets stiffer. More compliant structures pull out of plane to relieve some residual welding stress. Stiffness can be increased by using stronger base materials, using thicker sections, bracing strategic locations in a weldment, and rotating members to maximize the impact of the moment of inertia on the structure. To minimize residual welding stress, welds must displace freely. It will be difficult, however, to design for minimum structural restraint at strategic bracing locations. While the location of structural brace points may appear obvious, Figure 4 illustrates why the effect of joint restraint on material yield strength, in an environment of shifting Young’s Moduli, imposes strains on the weldment not easily anticipated. While the structural members respond to the effects of heating in a predictable manner, the unique fabricating history of each part and the structural configuration that comes together at each connection determine the final combination of stress and displacement that remains welded in the joint.

Each thermal region described in Figure 3 acts within its own regime against the shifting thermal gradients to increase residual welding stress. In the super-heated zone of  $L_3$  the weld metal pulls locally against the surrounding base metal contracting in all three planes as it cools. Connection members bend and twist regionally in the hot zone at  $L_2$  from the local heating and residual processing stress. Displacement in zone  $L_2$  is difficult to predict but ultimately affects stress at the finished weld. Globally at  $L_1$ , the geometry and design properties of the fixed structural frame restrain the dynamic regions of  $L_2$  and

$L_3$  from free displacement. The cumulative effects of joint restraint, joint design, and welding heat determine the eventual combination of connection displacement and residual stress that results.

Joints become highly restrained as assembly sequences increase the rigidity of a jumbo-shaped truss. The free-body diagrams shown in Figure 5 illustrate the increasing rigidity in a welded frame. A single pass weld shown in diagram (a) and joining thin, unrestrained members causes the smallest amount of residual welding stress to remain in the weldment. Thin sections warp and twist to relieve most of the added stress. These sections are not discussed in the present experiments but are considered unrestrained joints. The first boundary condition of the experiment is observed as a few weld passes

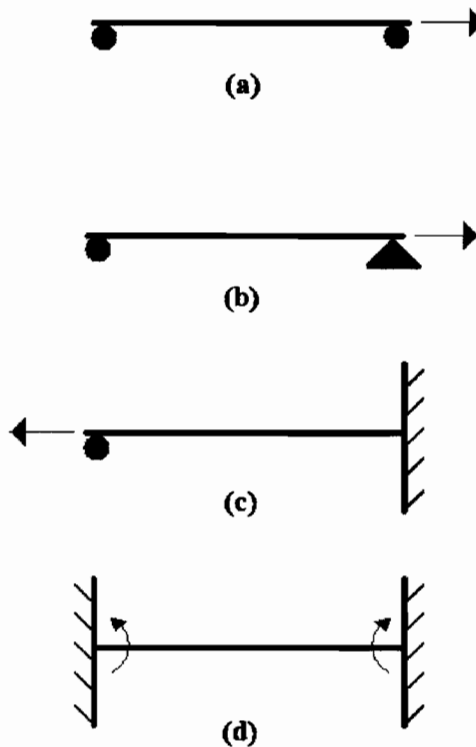


Figure 5. Free-Body Diagrams of Welded Rigidity

stack up and the weld joint locks up. The joint is locally restrained from displacing by the solid, intermediate weld passes. Diagram (b) in Figure 5 describes the Boundary 1 condition, a pinned connection under increasing welding stress. Internally, this connection is under medium joint restraint. Externally, the connection freely returns to its original location in the structure after cooling to ambient temperature, several hours after welding is completed. The regional shifting of connection members under residual heat may add additional restraint as they cool, but there is relatively little global restraint from the structure at Boundary 1.

The second connection node, on the opposite chord of the truss or second column of a moment-resisting frame, represents the fully restrained, Boundary 2 condition in the present experiments. Diagram (c) in Figure 5 illustrates a closing seam that initially is free to displace longitudinally. This freedom accommodates the members in thermal region  $L_2$ , shifting under preheat and residual welding heat. The completed Boundary 1 connection node, however, restrains the closing connection regionally and globally. The initial closing weld passes lock up the second joint locally, as happens during medium joint restraint of Boundary 1, but the stresses induced by thermal displacement remain as the closing seam cools to ambient temperature. The entire connection remains pulled out of its global position in the structure by the rigidity of the frame. Diagram (d) in Figure 5 describes the Boundary 2 condition after welding is complete. It identifies how the hot, liquid weld reacting in a rigidly fixed connection can increase the residual stress in the structure.



### 1.5.2. Local Joint Restraint

AWS developed several equations estimating the local displacement from shrinking welds. Blodgett proposed Equation 5 in the 1960s to estimate weld shrinkage transverse to the direction of welding (Blodgett 1976). This simple equation quantified the estimated displacement as a percentage of the final weld face width.

$$\Delta_{trans} = 0.10 \frac{A_{weld}}{t} \quad (5)$$

where  $A_{weld}$  = cross sectional area of weld;  $t$  = thickness of joint ; and

$\Delta_{trans}$  = transverse shrinkage.

AWS modified the Blodgett equation as Equation 6 in 1987 (Masubuchi et al. 1987). The new equation doubled the shrinkage estimated by the Blodgett equation and included additional displacement of 5% for the shrinking of the root gap. The present joint configuration was predicted to shrink 10 mm (0.41 in), though this was never observed during the experiment. The experimental joint configuration typically contracted 3 mm to 5 mm (0.12 in to 0.18 in), less than 45% of the displacement estimated by AWS, and 95% originally estimated by Blodgett. The percentage difference from the Blodgett equation would have increased if larger groove angles had been employed during the present experiments.

$$\Delta_{trans} = 0.2 \frac{A_w}{t} + 0.05d \quad (6)$$

where  $A_w$  = cross sectional area of weld;  $d$  = root opening;  $t$  = thickness of joint; and

$\Delta_{\text{trans}}$  = transverse shrinkage.

AWS also developed Equation 7 to estimate the contraction along the longitudinal axis of the weld (Masubuchi et al. 1987). The equation relates the longitudinal shrinkage displacement with the heat input from the welding current. Displacement is predicted to increase with higher amperages. Conversely, displacement decreases as the section thickness increases. The amperage parameter in Equation 7 captured the welding effects on the base metal. Displacement is very restricted along this axis, regardless of section thickness or amperage. Using 400 amperes observed while welding the experiments, the total predicted longitudinal displacement for the experiment joint is 0.09 mm (0.004 in).

$$\Delta L = \frac{C_3 IL}{t} 10^{-7} \quad (7)$$

where  $C_3 = 12$  or  $305$  when  $L$  and  $t$  are in inches or millimeters, respectively;  $I$  = welding current, amperage;  $L$  = length of weld;  $\Delta L$  = longitudinal shrinkage; and  $t$  = joint thickness.

The potential for displacement transverse to the weld axis is almost five times greater than the displacement longitudinally along the weld. High residual tensile stresses develop along this weld axis. The longitudinal axis is the second axis of the joint predicted to be in tension after welding.

The section thickness restrains the shrinking weld. Thin sections readily displace through their thickness to shed stress. As the sections get thicker, however, displacement is increasingly restrained. After the Northridge earthquake in 1994, The SAC Joint Venture with the Federal Emergency Management Agency, the American Institute of

Steel Construction and the National Institute of Standards and Testing studied base metal ductility requirements. As part of the tests, efforts were made to characterize the mechanical response of the moment frame beam-to-column connection. Dexter et al. (2002) loaded full section moment-frame welded connections to verify that the structural wide-flange shapes were suitable for seismic design. They observed no displacement of material through the thickness of the column flanges. They concluded that the geometric restraint at the connection drove the apparent yield and ultimate tensile strengths so high, that the beam would plastify long before the section would tear apart at the column.

They used 690 MPa (100 ksi) class weld filler metal to join the sections. The stronger weld metal forced yielding to occur in the weaker structural shapes. Tellingly, Dexter et al. (2002) observed no lamellar tearing in the experiments. Dexter's observations identify a weld zone completely restrained through the column flange thickness. Joint restraint through the section thickness creates tensile residual welding stresses in the third plane of the structure. Others have recognized the correlation between an increase in section thickness with an increase in residual welding stress (Masubushi et al. 1987, p. 238). Because little or no displacement will occur through the section thickness or longitudinal axis of the joint, transverse welding displacement offers the best opportunity to relieve welding stresses in the connection because the majority of displacement takes place transverse to the direction of welding.

### 1.5.3. Regional Joint Restraint

Regionally, the fixity of the weld joint changes while welding. The application of preheat and welding heat shapes the members in the weld zone as shown in Figure 3 and Figure 4. Equation 3 illustrates why the structural member expands and displaces during

heating of the  $L_2$  region. Only a discrete portion of a structural member is affected by thermal displacement, however. The surrounding  $L_1$  region at ambient temperature is not affected. A column or truss chord, heated along one flange, bends the entire member toward the applied heat as the affected flange increases in length. The length of the affected flange increases as the connecting beam gets deeper or the connection region gets longer. Connections can be large. The T-K-Y connections in the long-span trusses examined in this thesis were more than 914 mm (36 in) long.

AWS observed that most joint displacement occurs after the weldment has cooled down to relatively low temperatures. Actual weld shrinking accounted for no more than 10% of the overall displacement (Masubuchi et al. 1987). The present experiment observed this phenomenon, too. This thermal displacement of the connection is not to be confused with displacement that takes place during flame straightening. Flame-straightening heats may be applied at many spots along a member to physically upset the metal into a new shape. But each flame-straightened spot is a localized application of heat, applied for a short period of time. The thermal effects of a few, short bursts cannot be compared with the deep heat soaking associated with welding and preheat.

Regardless of the exact point of maximum  $L_2$  temperature, the surrounding base metal is thermally expanded. An increase in the weld area builds up more heat in the connection. Though weld heat input varies from pass to pass, heat distribution grows increasingly uniform through the base metal the more weld passes are made. As many as 40 passes were needed to fill the 50.4 mm (2 in) thick joints of the present experiment. Metal far from the welding arc shrinks imperceptibly. Metal within inches of the arc shrinks dramatically as the  $L_3$  heat is pulled through the  $L_2$  region by the  $L_1$  steel.

Welding and construction Codes mandate thick steels be preheated before welding. Groups 4 and 5 wide-flange structural shapes are thick sections. Adjoining members are heated to 66° C (150° F) or higher before welding. Seismic design mandates 177° C (350° F) as the minimum preheat temperature. Welders are required to maintain this minimum preheat temperature during all welding operations for at least 76 mm (3 in) around the welding arc. Enough residual heat was stored in the present experiment connection during welding to maintain weld interpass temperatures at approximately 204° C (400° F) without applying additional preheat. Welding begins within minutes after the weld zone reaches minimum preheat temperature. Any displacement from preheating is quickly incorporated into the overall displacement from welding and residual heat.

Considered application of preheat can compensate for regional displacement. Preheating the far-side flange, away from the weld, bends the column away from the welding heat. The column is bent away from the joint. Welding heat pulls the column through the prepositioned thermal displacement to straighten the column. Without the extra preheat, the weld predictably pulls the column off the centerline axis. In practice, preheating the far flange is not performed and is difficult to accomplish with uniform results. Structural members welded following conventional practice predictably vary from the ideal centerline axis.

Just as the residual heat from welding the beam flanges preheats welding of the beam web and connecting column or chord, welding the first stem of a T-K-Y truss node will preheat part of the second stem in the connection cluster. Welding the second stem maintains the heat in a portion of the first stem and preheats the third. Welding the third stem maintains heat in a portion of the second stem while allowing the first stem in the

cluster to cool. Regional heating displacement ripples through the connection as preheat and welding progress.

#### 1.5.4. Global Joint Restraint

The geometry of the structural frame, external to the shrinking weld and shifting weld joint, is the primary source of joint restraint (Masubuchi et al. 1987). The  $L_1$  frame is at ambient temperature and experiences no thermal displacement. Fixed connections far from the weld will pin those joint members to restrain their potential movement. Other intersecting members progressively stiffen the connection as each member is welded into place. The design rigidity of the connection has the greatest impact on residual welding stress. The residual stress in the connection increases as it is increasingly restrained by the structure. This global restraint has little influence on the stress distribution through the either connection or the structure (Masubuchi et al. 1987). Global joint restraint acts like a system of transverse springs through the welded members. The rigidity of this spring system expresses the degree of restraint.

## 2. EXPERIMENTAL PROGRAM

### 2.1. The Structural Bounds of the Beam-to-Column Welded Connection

Two welds are required to join a beam between two adjacent columns. The joint configurations are identical on each end and only the root gap will vary. The level of restraint imposed on the joints, however, is completely different. The first welded joint is made while the opposite end of the beam is free to move longitudinally. The second, closing joint is made with its opposite end completely fixed in the structure during welding. The first weld experiences the local effects of the shrinking weld. The second weld experiences the local welding effects and the additional resistance from the overall structure. The heat of the electric arc provides the driving force and the structure provides the reaction to create residual welding stress during fabrication of welded structures. This is the common model of welding stress described in AWS and other engineering literature.

Significant displacement in the connection outside of the shrinking weld is observed during welding of the present experiments. As more and more weld passes were laid into the weld joint, the temperature of the connection increased. The connection warped and twisted from thermal expansion as the overall heat input increased and the weld progressed. How these forces affect the final weldment depends upon many factors. Thermal displacement can either compound or alleviate the residual welding stress in a connection depending on how it occurs.

The energy of the welding arc and preheat activities create a thermal gradient

within the structure. The present experiments identify three components of welding restraint. Local restraint within the shrinking weld, regional restraint resulting from thermal displacement in the connection, and global restraint from the surrounding structural frame geometry combine to restrict displacement and reduce stress shedding. These restraint regimes expand upon the commonly considered source of residual welding stress, the shrinking weld. The restraint regimes correspond to regions along the thermal gradient. Local restraint begins directly beneath the arc where steel is liquid at  $1482^{\circ}\text{C}$  ( $2700^{\circ}\text{F}$ ) and extends outward to the point where steel regains minimum structural strength, at  $732^{\circ}\text{C}$  ( $1350^{\circ}\text{F}$ ). In multipass welds, the initial weld layers quickly combine to lock the joint in place and resist the balance of the shrinking weld. From the point where steel regains its strength, until the point where ambient temperature is reached, regional thermal displacement induces stresses into the connection after welding is completed. Finally, the surrounding structure at ambient temperatures globally reacts against local and regional displacement in the weld and connection region. These three regimes combine to react against the heat of the electric arc.

#### 2.1.1. Boundary Condition 1 – Medium Joint Restraint

The first welded connection in the frame is essentially unrestrained. The joint is tacked together prior to welding. Back-up bars are tacked to the column to support the molten weld while permitting the beam to slide as the weld shrinks. With the far end bolted finger-tight, the beam is free to displace longitudinally along its axis. The weld starts shrinking as soon as the welding arc passes and the weld begins to cool. The shrinking weld pulls against the column along the axis of the horizontal beam and the far-end root gap increases.



This connection could be considered a low restraint condition were the joint in a thin section with only one or two weld layers. The welds in thicker sections have sufficient interpass weld thickness to resist joint displacement. As the weld layers build up, they eventually stop the joint from shrinking. Welders frequently weld large root passes and large fill passes to lock the joint in place. These welds shrink more initially because of the high weld heat and deposition rates. But this technique reduces overall shrinking in the weldment after the joint is sufficiently filled to resist further welding displacement (Masubuchi et al. 1987). There is a trade-off between the dimensional integrity of the structure and the residual welding stress in the connections. Each time heat is applied to a thick joint, the connection must displace or the strain remaining in the joint must increase.

As many as 11 weld layers, made in over 40 weld passes were needed to completely fill the joints in the thick, jumbo sections used in the present experiments. Because the warm, solidified initial weld layers prevent displacement, the strain gauge data will record increasing strain induced in the connection. This restraint is localized at the weld because free displacement through the joint can no longer take place. Globally, the connection is relatively free to move back to its original location without adding further strain to the structure. These connections identify Boundary 1, medium joint restraint.

#### 2.1.2. Boundary Condition 2 – High Joint Restraint

The second connection in the structural frame is fully restrained. The far end of the beam is now completely welded and fixed into the stiff column by the first connection. The beam no longer slides freely along the erection bolts. The adjacent

column and the previously welded frame components resist the shrinking closing weld. The frame is too stiff to bend easily in compliance to the contracting weld. The ductile weld filler metal readily stretches at elevated temperatures. But by the time the steel has cooled to approximately 177°C (350°F), it has regained almost 85% of its room temperature yield strength. No stretching can take place and almost all of the welding stresses will remain in the welded frame when this joint is completed. Only yielding of the structure, fracture, or additional thermal stress-relieving operations will relieve residual welding stress.

Residual stress after welding has generally been assumed to approach the material's yield strength at room temperature (Lincoln Electric (1994); Masubuchi et al. (1987)). That assumption is probably valid for thin sections, approximately one-inch thick or less. Through-section thickness of thin material does not restrain displacement from stretching or necking. In-service loading can exert sufficient force to cause local yielding of the connection material and reduce residual stresses to negligible values during service life. Welding procedures can be crafted to temper each successive bead. The yield strength of steel decreases as the metal temperature increases until at approximately 454°C (850°F), it approaches a lower limit. At temperatures above 732°C (1350°F), steels rapidly lose their structural strength (ASTM 1972). Tempering weld beads and "wash passes" allow the underlying beads to stretch slightly, permit entrapped hydrogen to exhaust, and refine the resulting weld metallurgy. But the present experiments indicate the cooler weld layers limit stretching; improvement to weld metallurgy only ensures the weld performs as designed.

The shrinking weld locally sheds stresses exceeding the yield strength into the hot

center of the solidifying weld. The welding arc creates a thermal gradient from thermal region  $L_3$  to  $L_1$ . Region  $L_3$  includes not only the liquid weld metal, but also the metal immediately beneath the welding arc experiencing temperatures exceeding  $732^{\circ}\text{C}$  ( $1350^{\circ}\text{F}$ ), where steel loses its capacity to resist a load. Portions of the previously solidified weld layers will stretch and shed their contribution of residual stresses (Evans and Bailey 1997). All of the weld passes except the last one receive some weld tempering. The final weld pass is not typically tempered in production unless special welding techniques are followed. The final weld layer is a combination of stress-relieved and as-welded weld metal.

The expectation that residual stress approaches the material yield strength has little relevance to the designer unless joint restraint is considered. Experiments at Lehigh University (Blodgett 1998) showed the apparent yield strength of the connection increased as the level of restraint increased. Higher yield strength is gained by a reduction in joint ductility. The connections of 345 MPa (50 ksi) yield strength moment frame members can have an apparent yield strength as high as 690 MPa (100 ksi) due to the restraint inherent in the beam-to-column connection (Blodgett 1998). At high levels of restraint, the stress needed to get the connection to yield is greater than the ultimate tensile strength. Triaxial stress may cause the connection to fracture catastrophically with little or no ductile bending or tearing.

The displacement of a member due to an applied point load anywhere along its length is described in Figure 6. The displacement is calculated using Equation 8 (AISC 2005). For these experiments, this load is the result of a shrinking weld. The equation can be rewritten to calculate the stress of the contracting weld displacing the columns in

highly restrained connections. The stress applied through the joint is calculated by dividing this load by the area of the column. This is the residual stress from welding.

$$\Delta L = \frac{Pa^2 b^2}{3EI_{col}L_{col}}; P = \Delta L \left( \frac{3EI_{col}L_{col}}{a^2 b^2} \right)$$

$$\Rightarrow \frac{P}{A_{col}} = \sigma \quad (8)$$

where  $A_{col}$  = Area of column;  $E$  = Young's modulus,  $\sigma/\epsilon$ ;  $I_{col}$  = Second moment of an area;  $L_{col}$  = Length of column;  $\Delta L$  = Displacement;  $P$  = Load;  $a$  = Distance<sub>1</sub> along column axis;  $b$  = Distance<sub>2</sub> along column axis; and  $\sigma$  = Stress.

The beam-to-column connection is called a “moment” weld when it is designed to withstand significant inelastic distortions applied during a seismic or ballistic event. Structural steel wide-flanges can resist these forces. The “I”-beam shape of the wide-flange effectively resists bending through efficient placement of the section mass around the center of gravity. Wide-flange sections, categorized by size and weight per foot, get stiffer as they get heavier per foot. The producing mills roll flanges thicker to get more steel at the outside fiber of the section. This practice increases the overall depth of the

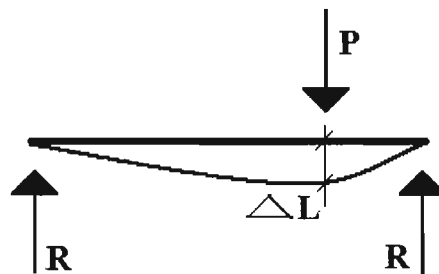


Figure 6. Simple Beam - Concentrated Load

section and increases the second moment of inertia,  $I$ . The second moment of inertia reflects the column's capacity to resist bending and deflection. The tensile welding stresses react against the stiff columns to impart a load at a point along the longitudinal axis of the columns. For this experiment, the point is located at the intersection of the centroid of the beam to the column flange over the centerline of the column web. This point is identified as  $\bar{y}$  in Figure 7. The location of the applied load determines the amount of deflection in the columns.

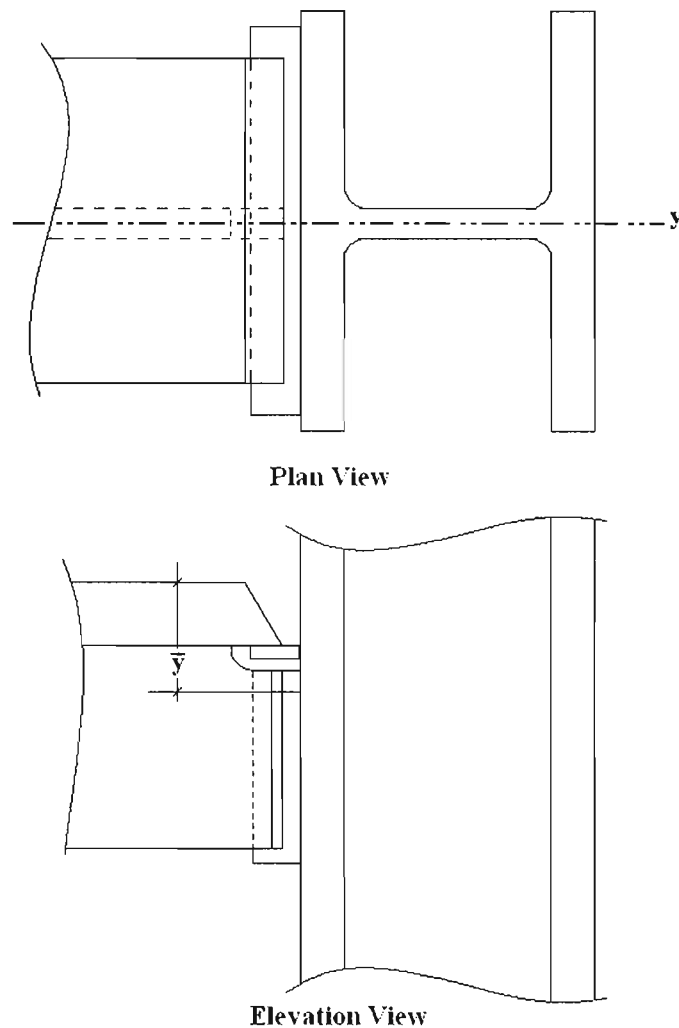


Figure 7. Location of the Applied Load

### 2.1.3. Analysis of Joint Restraint in Long-Span Trusses

The structural performance of a welded panel or space truss depends upon the alignment of the intersecting truss members. The truss provides a special case in structural analysis. By definition, the force in a truss member remains uniform along the members and moments within the truss are essentially zero when the joints are pinned. Excessive deformation of truss members and fixity at the joints will permit bending forces to develop in the structure. The increasing p-delta effects of the member displacement amplify the effects of any bending moments. The shrinking welds cause the members to behave as though they had been installed short into the truss, pulling the connection out of plane and inducing additional forces.

The final alignment of the welded connection relative to the maximum allowable tolerances established by AWS and AISC can be anticipated using the displacement data from the present experiments and structural analysis. The method of virtual work makes calculating welding displacement of key truss panel points possible. But, because of the restraint inherent in truss connection nodes, most of the expected displacement will be realized as increased residual welding stress.

Trusses are structurally indeterminate. They are rigid bodies with limited degrees of freedom (DaDeppo 1999). The method of virtual work is a virtual energy method utilizing the principle that the work of all forces and arbitrary displacements away from the applied force configuration must be zero for a system that is in equilibrium. For Newtonian bodies conforming to Hooke's law, the work created by external forces on a system equals the work created by internal forces within the system. The designer can impose a virtual internal force to the truss to produce a virtual displacement. The

experimental displacement data from the present experiments are incorporated into the equation to calculate a comparable change in length in the actual welded structure.

Virtual work can be compared mathematically to the work displacing the truss members during welding. Analyzing the load path of forces through the truss joints enables calculation of the potential truss displacement at the point of applied virtual force. The equation for virtual work is simplified in Equation 9 to calculate the virtual displacement at a given connection node in a truss.

$$u = \sum_m n \Delta L \quad (9)$$

where  $\Delta L$  = change in length;  $n$  = virtual load,  $m$  = the index of summation, and  $u$  = virtual displacement.

The method of joints offers a simple technique to develop load paths through the truss. The magnitude of forces through the truss relative to one another is calculated employing an understanding of zero-force members and trigonometry. The virtual load,  $n$ , in the truss members is determined by structural analysis. The virtual load acts along the length of the specific member to perform work. Once the virtual relationship between load and length are determined, the relationship can be applied to calculate displacement in the actual truss connection. Calculating the virtual work done by cooling connections through the truss will determine the resulting welding displacement. Actually, there will be very little displacement in the truss connections because they are highly restrained. The resulting residual stress can be calculated using Equation 10.

$$\Delta L = \frac{PL_{Beam}}{EA_{Beam}}; \sigma = \frac{P}{A_{Beam}} = \frac{E\Delta L}{L_{Beam}} \quad (10)$$

where  $A_{Beam}$  = Area of beam;  $E$  = Young's modulus,  $\sigma/\epsilon$ ;  $L_{Beam}$  = Length of member;  $\Delta L$  = Displacement;  $P$  = Load; and  $\sigma$  = Stress.

#### 2.1.4. Case Study – Long-span Trusses

Current building design incorporates long-span trusses to support the roofs and floors covering wider and wider open spaces. Figure 8 shows a section of a long-span truss. It details the structural members and is the basis for the analysis in this thesis. Complete penetration welds joined jumbo wide-flange shapes in this example to support an “aqua” theater. Three 34.7m (114 ft.), Pratt-type truss panels weighing as much as 145.1 Mg (160-tons), were supported between W360 x 463 (W 14 x 311) supporting columns. The huge size of the trusses necessitated assembly at the jobsite. Shop cranes were not available in the region to pick up the sections for shop assembly and the truss segments were too heavy to ship.

The joints between the chords and the chord-to-panel members were the same single-bevel groove weld configuration used in the present experiments. The field weld joints were cut to 45 degrees and required more weld filler metal. Over 8.1 kg (18 lbs) of weld filler metal were used to fill one flange joint alone. The long-span trusses differed from the present experiments in that the diagonals and webs were joined to the toes of the chord flanges, not across the flange face like a moment frame. The residual welding stresses in the long-span truss are applied in the y-axis of the chord member, bending the section along its weakest axis.





Welders are responsible for the fabrication accuracy of a welded truss. Erectors use cables, bolts, guy-lines, and temporary restraints to install trusses and pull frame assemblies within AISC erection limits (AISC 2005). Erection stresses are applied globally to the frame and get fixed into the frame by welding. These techniques further restrict displacement and contribute to the high degree of restraint. AWS imposes assembly limits when welding trusses (AWS 2008). To comply with the AISC Code, truss chord centerlines may not vary by more than 32 mm (1-1/4 in) from true alignment over the 34.8 m (114 foot) length of the long-span trusses. The trusses were welded to supporting columns during welding. AISC (2005) establishes the maximum allowable deviation from column section centerline as 1/500 of the overall length or +51 mm / -25 mm (+2 in/-1 in), whichever is smaller. Tolerances increase after the 20<sup>th</sup> floor of a building and greater deviation is permitted for columns greater than 13.7 m (45 ft) tall. Steel producers roll wide-flange sections within specified limits, too (ASTM 2005). The camber and sweep of column sections can vary out of true plane by as much as 9 mm (3/8 in) and still be acceptable. Analysis of the trusses illustrates the trade-off between structural dimensional integrity and structural strength.

## 2.2. The Test Assembly

The present experiment test assembly simulates the connections in the AISC prequalified Special Moment Frame. These connections are routinely used in the construction of seismic resisting structures and long-span trusses. The experiments employed short spans and jumbo sections to exaggerate the joint restraint and maximize the welding stress in the two-bay frame assembly. Figure 9 describes the test frame assembly and identifies the various gauge locations. The axis of the weld joint is

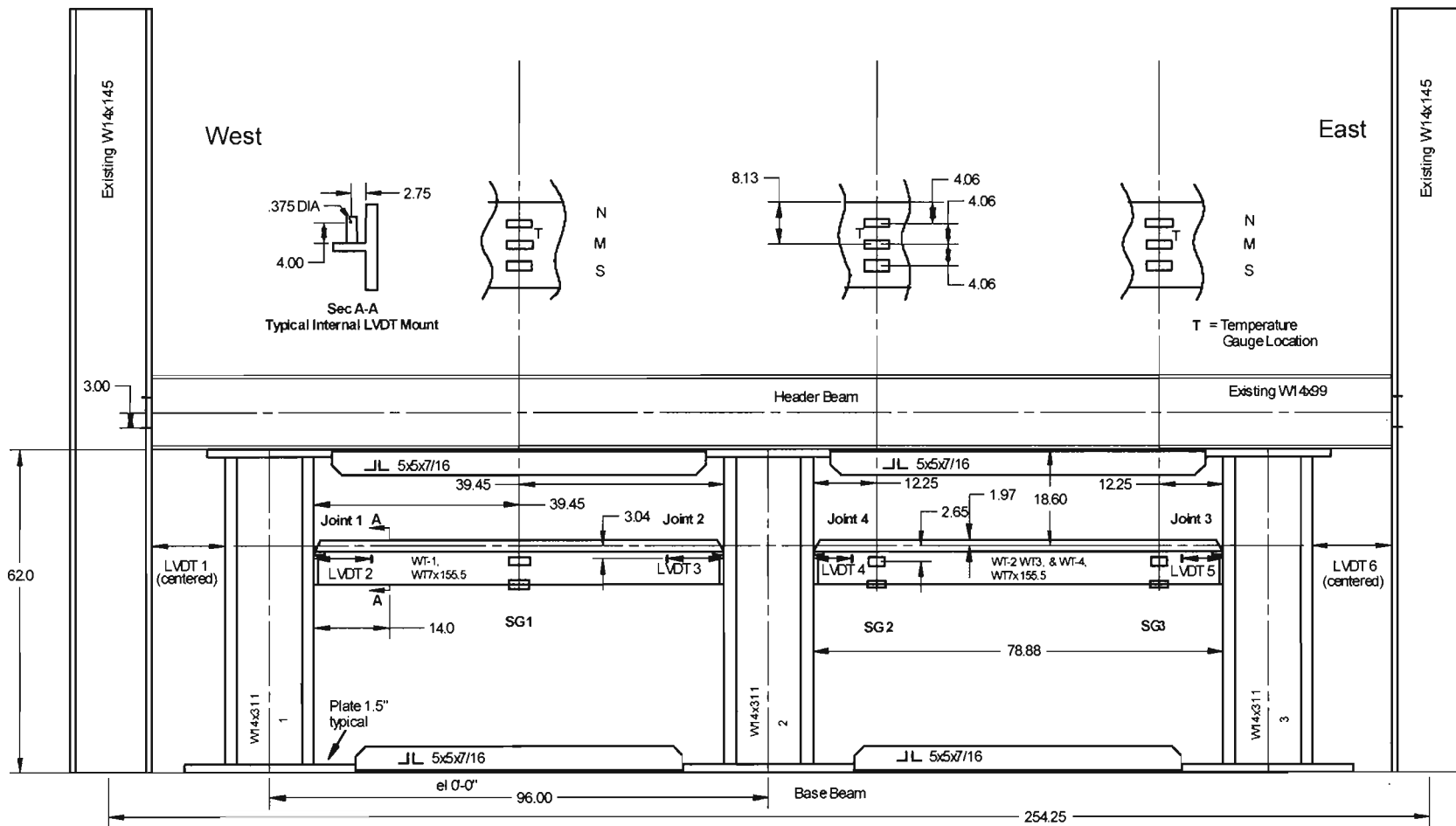


Figure 9. Test Frame and Gauge Locations

transverse to the longitudinal direction of the test assembly. The experiments were measured along the longitudinal axis of the test assembly. Weld shrinkage equations in 1.5.2 predict that shrinking through the joint, transverse to the direction of welding, will be more than 1000% greater than shrinking parallel to the weld axis or the through-section axis.

The test frame configuration was developed to restrain the weldment from displacing longitudinally and transversely during welding. The rolled, wide-flange structural shapes conform to ASTM A992 and ASTM A6, group 4. The short, stubby columns were fabricated from W360 x 463 (W 14 x 311), wide-flange sections. The flanges of these sections are approximately 57 mm (2-1/4 in) thick.

The beams were fabricated by cutting wide-flange sections in half through their web to form T-sections, WT 180 x 213.5 (WT 7 x 155.5). Double angle-iron stiffeners were wedged between the top and bottom baseplates to prevent the columns from slipping. The columns and the stiffeners were bolted into the structural test frame with fully tensioned A490 and A325 fasteners. Even with all of these precautions, we were unable to completely fix the columns to the structural test frame. Steel mills carefully control the chemical and mechanical properties of modern wide-flange shapes to facilitate joining by welding. They control the steel chemistry to maintain a relative low carbon equivalent.

The carbon equivalent is a measure of the steel's susceptibility to cracking during welding. The mills have recently specified a ratio of material yield strength to ultimate tensile strength. Older steel specifications permitted minimum yield strength with no maximum tolerance limits. These older steels were generally much stronger than

designers expected. Higher actual strength precluded the material from yielding safely before cracking. Designers expected common ASTM A36 mild steels to yield at stress levels as low as 248 MPa (36 ksi). Actual test results showed older steels will not yield until the test stress exceeded 345 MPa (50 ksi). They were routinely dual certified by the mills to meet both ASTM A36 and the much stronger ASTM A572 grade 50.

The weld joint in a beam-to-column moment weld is a unique combination of intersecting rolling orientations and dissimilar mechanical properties. These intersections are shown in Figure 10. Beams, rolled longitudinally, are welded to the outside through-thickness surface of the perpendicular column. Structural materials exhibit different mechanical strength and elongation values depending upon whether they are tested longitudinally, transversely, or through the section thickness. Tensile tests in the longitudinal direction are stronger than coupons taken in the through-section direction. Material strength also varies depending upon where the test coupon is obtained in the

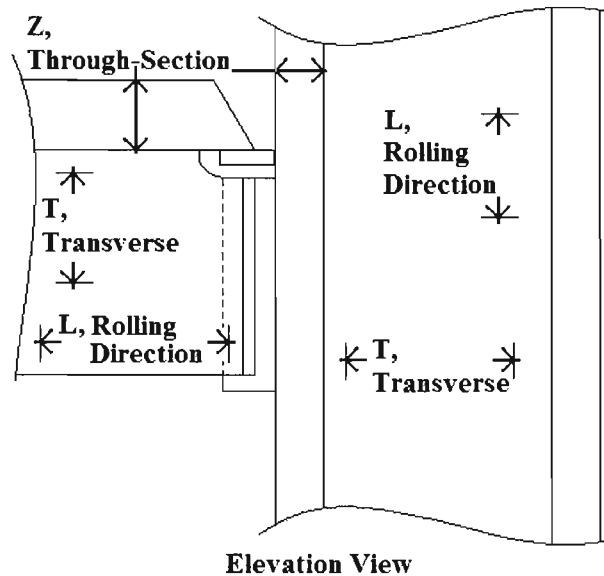


Figure 10. Rolling Directions

section. Standard ASTM test locations at the section flanges exhibit much higher strengths than the yield strengths measured in the web or the “k” zone at the web-to-flange intersection. Weld filler metal in structural connections are always stronger than the base metal. Thus, three different strength levels are present in each joint. The filler metal is almost 40% stronger than the A992 base metal. The mechanical properties of these materials are summarized in Table 1. They are obtained from test reports performed at the producing mill and from local mechanical tests.

During field installation, beams are installed between upright columns during building erection. The beams can be welded into the columns once the columns are plumb and anchored into position with guy-lines. Two beams are joined to each side of the first center or corner column to balance welding distortion. The welded ends of the beams lock each additional column in place as they are welded. The typical welding sequence completely welds out the flanges of the beam first, then the web (President Robert North, Ironworkers Local Union 27, personal communication, January 18 2004). Field joints are typically welded from only the top surface to minimize overhead welding. This configuration requires huge amounts of weld for jumbo shapes. The flanges of some jumbo shapes can reach 140 mm (5-1/2 in) in thickness. While welding the joint from two sides of the joint reduces the amount of weld filler metal by 50%, it is generally assumed that the additional welding time from one-side welding is offset by the lack of welders capable of successfully welding in the overhead position.

Table 1. Mechanical Properties of Materials

Description	Yield Strength	Ultimate Tensile Strength	Elongation in 51 mm (2 in)	Notch Toughness Impact @ Temperature
<b>A 992, Requirements</b>	<b>345 to 448 MPa (50 to 65 ksi)</b>	<b>448 MPa min (65 ksi min)</b>	<b>21% min</b>	<b>27 Joules @ 21°C (20 ft-lbs @ 70°F)</b>
A 992, material test reports, Flange	359 MPa (52 ksi)	490 MPa (71 ksi)	25%	226 Joules @ 21°C ave. (167 ft-lbs @ 70°F ave.)
A 992, material test reports, Core	359 MPa (52 ksi)	490 MPa (71 ksi)	27%	173 Joules @ 21°C ave. (128 ft-lbs @ 70°F ave.)
A 992, Test Frame Material, Flange	348 MPa (50.4 ksi)	507 MPa (73.5 ksi)	31%	267 Joules @ -7°C (197 ft-lbs @ 20°F ave.)
A 992, Test Frame Material, Core	369 MPa (53.5 ksi)	514 MPa (74.5 ksi)	30%	308 Joules @ -7°C (227 ft-lbs @ 20°F ave)
<b>A5.20, E71 T-8, Requirements</b>	<b>400 MPa min (58 ksi min)</b>	<b>483 MPa (70 ksi min)</b>	<b>22% min</b>	<b>27 Joules @ -29°C 20 ft-lbs @ -20°F</b>
E71 T-8, typical test certificate	462 MPa ave. (67 ksi ave.)	600 MPa ave. (87 ksi ave.)	26% ave	61 Joules @ -29°C ave. (45 ft-lbs @ -20°F ave.)
E71 T-8, AWS D1.1 welding procedure qualification tests	410 MPa ave (59.4 ksi ave.)	552 MPa ave (80 ksi ave)	31%	Weld Metal: 69 Joules @ -29°C ave (51 ft-lbs @ -20°F ave.) Heat-Affected Zone: 130 Joules @ -29°C ave (96 ft-lbs @ -20°F ave)
E71 T-8, AWS D1.5 welding procedure qualification all-weld metal tests	523 MPa ave (75.7 ksi ave)	610 MPa ave (88.4 ksi ave)	22%	All Weld Metal: 71 Joules @ -29°C ave (52 ft-lbs @ -20°F ave)

### 2.3. The Beam-to-Column Weld Connection

The welding for all joints attempted to comply with the requirements of AWS (2008). The welding procedure specification used to join the beam-to-column joint is prequalified by the structural welding code. The procedure is for a complete penetration, bevel groove joint, complying with figure TC-U4a-GF. The welding procedure specification permits the chamfer angle of the joint to vary between 30 and 45 degrees. A larger angle improves the welder's view of the root of the weld, but increases the amount of filler metal required to fill the groove. A steel backup bar is tack-welded to the bottom,

root side of the joint to support the liquid weld metal flowing into the joint gap between the beam and column. This root gap can vary between 5 mm (3/16 in) and 16 mm (5/8 in), in accordance with the upper and lower tolerance limits established by the welding procedure specification. The joint configuration controls the number of welding passes needed to completely fill the joint. A 30-degree bevel angle was selected for the experiments to reduce the amount of weld filler metal required to fill the joint. The shop fabricated bevel angles actually measured 32 degrees. The actual root gaps of the shop prepared welds varied between 8 mm to 17 mm (5/16" to 11/16").

Some exceptions to the Code were made to accommodate the actual conditions encountered for welding the web of the beam. The joint bevel was too narrow to be prequalified for the self-shielded filler metal used to fill the joint. This exception was made out of economic convenience. The narrow groove did not permit sufficient welder visibility to consistently make quality welds. Welding discontinuities in the web weld and the fact that only 102 mm (4 in) of the joint could be welded out reduced the balance of the residual welding stresses between the web and the flange.

The structural welding code establishes a 152 mm (6 in.) diameter circle surrounding the welding arc that must be controlled while welding carbon steels. AWS and AISC mandate that the entire weld zone must be maintained at or above established minimum preheat temperatures while welding. The preheat temperature specified for the thick sections used in the experiments was 66°C (150° F) minimum. It took approximately 15 minutes to preheat the joints during the experiments. No preheat was applied to the sections beyond the weld zone.

After preheating, residual heat from the welding arc collects in the structural



members while welding. Preheating the joint broadens the volume of metal above ambient temperatures. A large, preheated region slows down the welding quench rate and flattens the temperature gradient through the connection. If the base metal temperature gets too high, the temperature gradient from liquid metal to ambient temperature decreases and the weld quench rate is not sufficient to rapidly cool the weld. The rate at which a weld cools can be optimized to improve mechanical properties in the connection.

The welds joining WT-1 and WT-2 to the columns complied with AWS prequalified weld requirements. Preheat was applied and interpass temperature limitations were observed. WT-3 was welded following the same procedures as WT-2, except preheat was omitted. High heat input welding techniques were employed installing all WT. High heat techniques included maximizing amperage and voltage settings while slowing down the welder's speed of travel. This technique maximized the amount of weld metal deposited and maximized heat input introduced into the connection. Even with the high heat input technique, welding interpass temperatures never exceeded the welding procedure limits and welding progressed until the joint was completed.

Limiting weld interpass temperatures ensures the quench rate is fast enough to minimize the aging effect heat has on steel (Honeycombe and Bhadeshia 1995). Maximum interpass temperatures are imposed during welding to maintain adequate quench rates in the weld zone. Holding high strength, low alloy steels at elevated temperature for long periods coarsens the resulting grain structure reducing mechanical properties. Welding is routinely stopped to permit the weld zone to cool to 288°C (550°F) or below before welding starts again. Unless the weld zone is allowed to cool to 550° F, the joint will not draw heat out of the weld joint quickly enough to develop optimum

Charpy V-notch impact properties.

Codes impose upper and lower limits for electrical parameters that are determined to affect weld quality. Welding procedures describe those limits for welders who then tailor their personal techniques to comply with the governing code. The heat needed to successfully weld steel needs to be balanced against the potential for aging the metal with slower cooling rates. All welds in the present experiments were run with large, 2 mm (5/64 in) diameter electrodes at high amperages and voltages. Equation 11 describes the relationship of electrical parameters to welding travel speed in the weldment. Higher speed of travel used at high electrical parameters reduces the overall heat input into the joint during welding.

$$kJ / \text{unit length} = \frac{\text{Volts} \times \text{Amps} \times 60}{\text{Speed of Travel (unit length / minute)} \times 1000} \quad (11)$$

where J = Joules.

Some metals have a limited tolerance for welding heat. Grain structures change and constituent elements migrate. Heat input limits are specified when notch-toughness at near nil-ductility temperatures is of concern to the engineer. Weld filler metal is designed with special deoxidizers and other constituents to improve the mechanical properties of the resulting weld. Higher amperage melts more weld metal. It is beneficial to add as much filler metal to the weld as can be controlled while welding. Higher voltage increases the force of the metal moving across the arc. Slower travel speeds distribute the welding heat over larger areas. Establishing limits to all of these parameters controls heat input into the weld joint. In the present experiments, welders followed the welding procedure in Figure 11.

## AWS PREQUALIFIED WELDING PROCEDURE SPECIFICATION

Material Spec. <u>GR60/PS I &amp; II</u> Thickness <u>1/8" MIN.</u> Welding Process <u>FCM</u> <input type="checkbox"/> [Manual] <input checked="" type="checkbox"/> [Semi-Automatic] Position of welding <u>1G &amp; 2G</u> Welding Progression <u>N/A</u>	Preheat/interpass temperature IN: _____ °F								
Filler metal classification <u>E71T-8</u> Specification <u>AWS A5.21</u> Shielding gas type <u>N/A</u> Flow rate <u>N/A</u> Single or multiple pass <u>SINGLE/MULTIPLE</u> Post weld heat treatment <u>NOT REQUIRED</u> Welding current type <u>DC</u> polarity <u>STRAIGHT</u> [XEN] Backing <u>Group I or II back up bar</u> Backing gas <u>N/A</u> Notes: <u>The back up bar may be removed when required by contract.</u>	<table style="width: 100%; border-collapse: collapse;"> <tr> <td style="width: 60%;">UP THRU 3/4 [1]</td> <td style="width: 40%;">NONE</td> </tr> <tr> <td>OVER 3/4 THRU 1-1/2</td> <td>50</td> </tr> <tr> <td>OVER 1-1/2 THRU 2-1/2</td> <td>150</td> </tr> <tr> <td>OVER 2-1/2</td> <td>225</td> </tr> </table> <p>[1] WHEN BASE METAL TEMPERATURE IS LESS THAN 32° F, PREHEAT AND MAINTAIN AT 70° F MIN UNTIL WELD IS COMPLETED</p>	UP THRU 3/4 [1]	NONE	OVER 3/4 THRU 1-1/2	50	OVER 1-1/2 THRU 2-1/2	150	OVER 2-1/2	225
UP THRU 3/4 [1]	NONE								
OVER 3/4 THRU 1-1/2	50								
OVER 1-1/2 THRU 2-1/2	150								
OVER 2-1/2	225								

### WELDING PROCEDURE

SINGLE BEVEL GROOVE WELD T-JOINT  
T<sub>1</sub> & T<sub>2</sub>

FABRICATION PARAMETERS				
Passes as needed	Electrode Diameter	Welding Current		Speed of Travel (ipm)
		Amps	Volts	
1G & 2G	5/32"	145 - 400	19 - 27	8 - 20
Contact Tip to Work Distance = 1" ± .14"				
Variables	"	R	S	n
Minimum	1/8"	3/16"	N/A	30°
Maximum	Unlimited	5/8"	N/A	45°

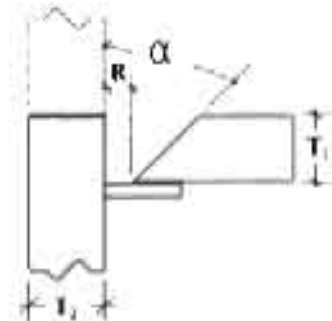


Figure 11. Welding Procedure

### 2.4. Location and Selection of Gauges

Gauges were located to measure displacement and strains in the longitudinal direction of the test frame. As discussed in 1.5.1, the majority of displacement due to welding occurs in this direction. Linear Variable Displacement Transducers (LVDT) were attached to the column centerlines along the X-axis. Strain gauges were attached to measure the strain across the beams while welding.

Figure 5 shows two LVDTs located between the existing W360x216 (W14x145)

structural test frame columns and the exterior W360x463 (W14x311) stubby columns of the test assembly, opposite the centroid of the WT beams. This is the location of maximum column bending and displacement from the welding cycle. Figure 9 shows four other LVDTs located 76 mm (3 in) below the centroid of the WT Beam at the column-to-beam connections. These gauges measured the displacement at the weld joints during the welding cycle. The interior LVDT were installed below the WT centroid to enable gauge installation. The centroid of the beam section falls within the flange of the WT. Figure 9 identifies each joint welded during the experiments. Once Joints 1, 2 or 3 were welded, their joint gaps did not change while the closing seams, Joints 2 and 4, were welded. For this reason, the LVDT at Station 2 was removed during the welding of WT-2 and never replaced.

Precision strain gauges measured the strain imposed on the structural test frame by the welding operations. Figure 9 shows three arrays of strain gauges attached to the WT beams, one array in the West Bay and two arrays on each beam end in the East Bay. Each array was comprised of five longitudinal strain gauges. The figure details three strain gauges attached along the top flange of the WT beam, running north to south. Another strain gauge was attached to the bottom of the WT stem opposite the gauges on the top flange. Finally, a fifth strain gauge was attached on the South face of the WT stem 67 mm (2-5/8 in) below the centroid to clear the fillet of the WT and facilitate gauge installation. Locating the gauges on the South face of the beam protected the gauges from welding heat and the molten slag generated during field preparation of Joint 4-2. General-purpose CEA-06-250UN-350 Vishay Micro-Measurements gauges were selected for their availability and compatibility with MTS data-logging software. The CEA gauges were

robust and could be used continuously from 204°C (400°F) to temperatures as low as –73°C (-100°F). All gauges were located to protect the soldered electrical connections from temperatures above 149°C (300°F).

Temperature gauges were added to the test frame during other experiment series, WT-4 through WT-6. They were located on the WT flanges, with the strain gauge arrays. The gauge at Station 1 measured ambient temperatures. Gauges at Stations 2 and 3 measured connection temperatures during welding. The data from these experiments were applied to the data gathered welding WT-1 through WT-3.

## 2.5. Gauge Correction

Data from the experiments were gathered over the course of a year and routinely stopped during the testing series. Each new file established its own zero point for strain, displacement, and temperature. To correct this recording error, the final, relevant value of the previous test was added to the apparent zero point of the current test. The data points of WT-1, Joint 2, at 14 hours were used to define the residual welding strains and displacements in the West Bay of the test assembly. They defined the starting points for LVDT #1, #2, and #3 and the strain gauges at Station #1 after the East Bay WT beam was removed or cut to prepare for Joint 4-2. Each gauge started recording at some low deviation from zero. This recording noise was removed from the data by subtracting the first datum recorded for the test from the recorded data for the experiment series.

Strain gauge data must be corrected for temperature to be accurate. Electrical resistance of the strain gauges varies not only with strain, but also with temperature. Vishay has published adjustment equations for their CEA strain gauges to calculate the thermal output of the strain gauge for variations in substrate temperatures (Vishay 2007).

The electrical resistance measured due to temperature change, thermal output, should be subtracted from the gauge reading to accurately describe the welding strains at elevated temperature. Data corrected with equations are not as accurate as data corrected with compensating, “Dummy” gauges. The correction, however, is sufficiently accurate to verify the strain from welding the structural frame. Vishay (2007) derives the thermal output equation from calibration data using carbon steel test blocks, AISI 1018. This steel alloy is chemically similar with the HSLA structural steel and the same thermal coefficient of expansion applies. The Vishay (2007) correction curve indicates that as the substrate temperature increases, the thermal output of the gauge increases.

The strain measurements at elevated temperatures can be corrected following the thermal output correction curves attached to the gauge certification. The curve shows the strain data can be roughly corrected by subtracting -100 microstrains from measurements taken from 93°C (200°F) to 149°C (300°F). These temperatures were approached at the gauges while welding the flange. This correction serves to increase the overall tension recorded during welding by approximately 100 microstrains and similarly decreases the compression. Thermal output is not applicable to the strains recorded at room temperature, however. The gauge adjustment curve goes to zero at room temperatures. The strains remaining in the frame assembly after several hours of equilibrium at ambient temperature define this experiment. No thermal output adjustments were made to these data.

## 2.6. Gauges in the Welding Environment

Experimental measurements were obtained in a very harsh environment. Molten spatter, hot chips of slag, and cycling of extreme temperatures challenged the installation

of the gauges. The welding process produces hot slag that must be removed by chipping. Molten droplets of spatter are spit out of the arc during welding. The carbon arc gouging operation sprays molten metal out of the joint with compressed air. The success of the experiments depended upon the installation of the gauges. They were installed and calibrated in accordance with the manufacturer's written practices and good workmanship.

Strain gauge locations were rough ground to remove mill scale and foreign material prior to installing the WT. The attachment spots were fine ground with a Dremmel rotary file to provide a surface suitable for gluing the strain gauges on the structural steel. The spots were dried with a hot-air gun before the adhesive was applied. The strain gauges were sealed with polyurethane. The sealer was allowed to dry for twenty-four hours before covering the gauge locations in RTV (room temperature vulcanizing) silicone waterproof sealant. The gauges were protected from the welding slag with ceramic tape capable of withstanding 593°C (1100°F) without burn through.

The location of the LVDT on the far side of the welding joints protected them from the heat and slag from welding. The LVDTs were removed during the cut out of WT-2, Joint 4-2 to protect them from burning slag. Metal shields were later installed to protect them. Even with all of the care taken during installation, gauges still failed. More discussion on individual gauges is given later in the analysis of gauge data.

## 2.7. Experiment Methodology

Four WT beams were welded between three columns during the experiments. Figure 9 shows the first beam, WT-1, welded into the West Bay with joints 1 and 2. The weld joints were named after their respective welding sequence. All subsequent welds

made in the test assembly were resisted by the fixed connections in the West Bay. Joint 1 joined the WT-1 to the West exterior column in a medium-restraint connection. Joint 2 joined the WT-1 to the center column in a high-restraint, closing weld connection. Three other WT beams were welded later into the East Bay in three more series of experiments. Joint 3 was made on the East exterior column as another joint under medium restraint. The final weld, Joint 4, was welded to the center column, maximizing the joint restraint at that connection. Joint 4 was cut out and rewelded as joint 4-2 in each experimental series. After welding all three joints, WT-2, WT-3, and WT-4 East Bay beams were cut out of the test frame.

Table 2 identifies each WT beam installed in the test frame and the level of joint restraint in each attachment weld. The table also describes whether the joint configurations were prepared in the shop or in the field during the experiments. Joints 3 and 4-1, the shop prepared joints, are fabricated with oxy-acetylene cutting machines. The dimensional attributes of the joints are tightly controlled and only the root gap between the end of the beam and the column varies. Joint 4-2, the field prepared joints, are prepared manually by carbon arc gouging out of the previous weld metal. The material was too thick to maintain strict AWS joint configuration tolerances. The included angles and root gaps of the manually cut joints were always larger than the shop prepared joints. Welding was performed with more weld filler metal to fill the larger groove area which added to the thermal effects observed during the experiments. Figure 12 illustrates the differences between shop and field prepared joints.



Table 2. WT Beam Schedule and Joint Restraint

<b>WT Installation Location</b>	<b>WT Number</b>	<b>Medium Restraint</b>	<b>High Restraint</b>	<b>Comments</b>
West Bay	WT-1	Joint 1 – Medium	Joint 2 – High	Shop prepared joint configuration
East Bay	WT-2	Joint 3 – Medium	Joint 4-1 – High	Shop prepared joint configurations
East Bay	WT-2	–	Joint 4-2 – High	Removed weld 4-1 and rewelded as weld 4-2; Field prepared joint configuration
East Bay	WT-3	Joint 3 – Medium	Joint 4-1 – High	Shop prepared joint configurations
East Bay	WT-3	–	Joint 4-2 – High	Removed weld 4-1 and rewelded as weld 4-2; Field prepared joint configuration
East Bay	WT-4	Joint 3 – Medium	–	Shop prepared joint configuration; Weld at Joint 3 performed to observe bowing of column from $L_2$ thermal effects during welding and equilibrium; Weld 4 not performed

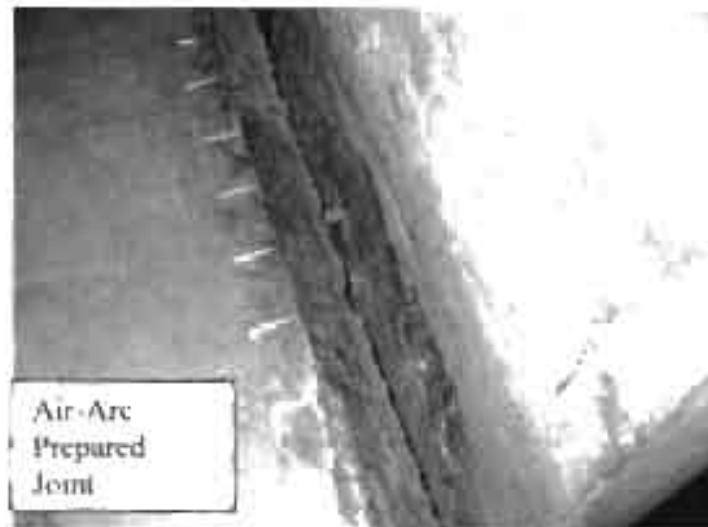


Figure 12 Typical Weld Joint Preparation

### 3. EXPERIMENTAL RESULTS AND DATA ANALYSIS

#### 3.1. General Considerations in the Data Analysis

Joints 1 and 3 are joints under medium restraint. Joints 2, 4-1, and 4-2 are highly restrained. The changing strain in the frame is recorded in the graphs of Figures 13, 14, 15, and 16. The changing displacement through the frame is recorded in the graphs of Figures 17, 18, 19, and 20. Thermal displacement after welding is complete is observed in all welds.

The gauge data of experiment WT-1, Joints 1 and 2, do not perceptibly change after the welds in this bay are completed. LVDT 2 and 3 stop displacing after the WT-1 welds fix the beam in place and provide no more information. They are removed from all subsequent analysis. LVDT 1 showed variations as large as 2.8 mm (0.11 in) while welding the highly restrained joints in WT-1 and WT-2. The LVDT changed less than 0.02 in) while welding WT-3. Gauge damage is the most likely cause of this loss of information. It is unlikely the column yielded under the welding stress. Other difficulties were encountered while collecting data. These difficulties resulted in other missing or misrepresented data. They are noted in the analysis below.

Strain versus Time  
WT-1, Joints 1 and 2, Station 1

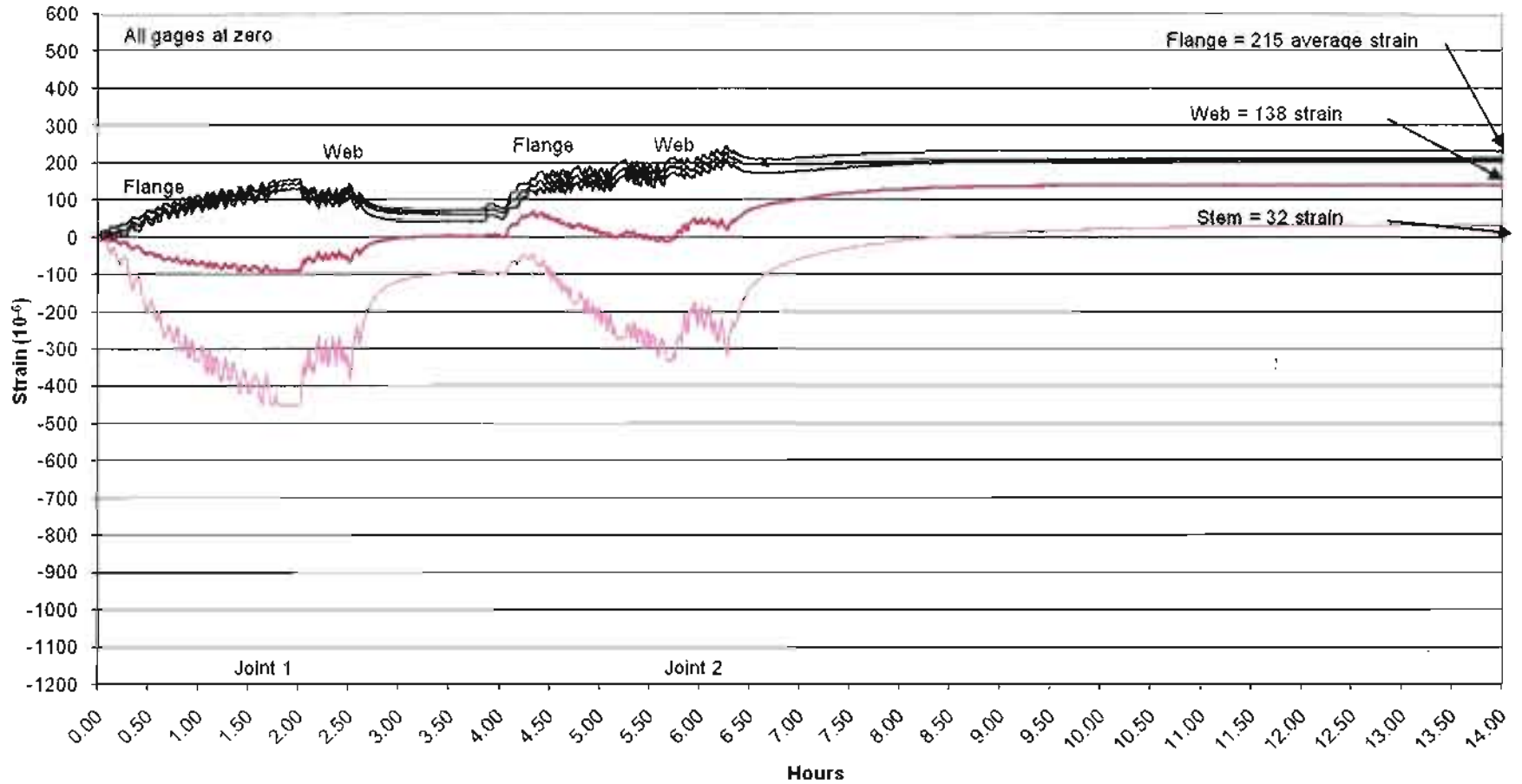


Figure 13. Graph - Strain Versus Time, WT-1, Joints 1 & 2

Strain versus Time  
 WT-2, Joints 3 & 4-1, Stations 2 (West) and 3 (East)

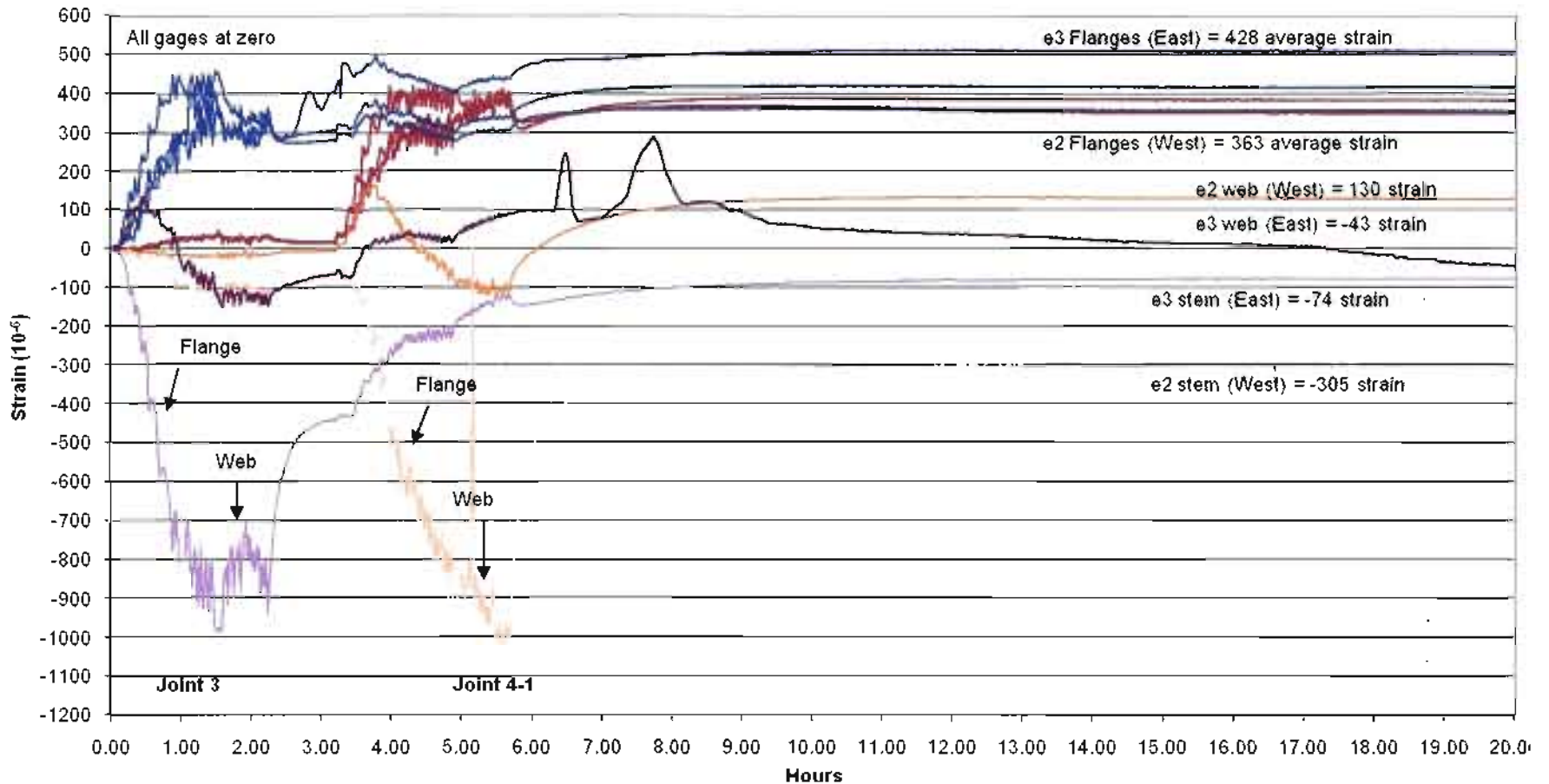


Figure 14. Graph - Strain Versus Time, WT-2, Joints 3 & 4-1

Strain versus Time  
 WT-3, Joints 3 & 4-1, Stations 2 (West) and 3 (East)

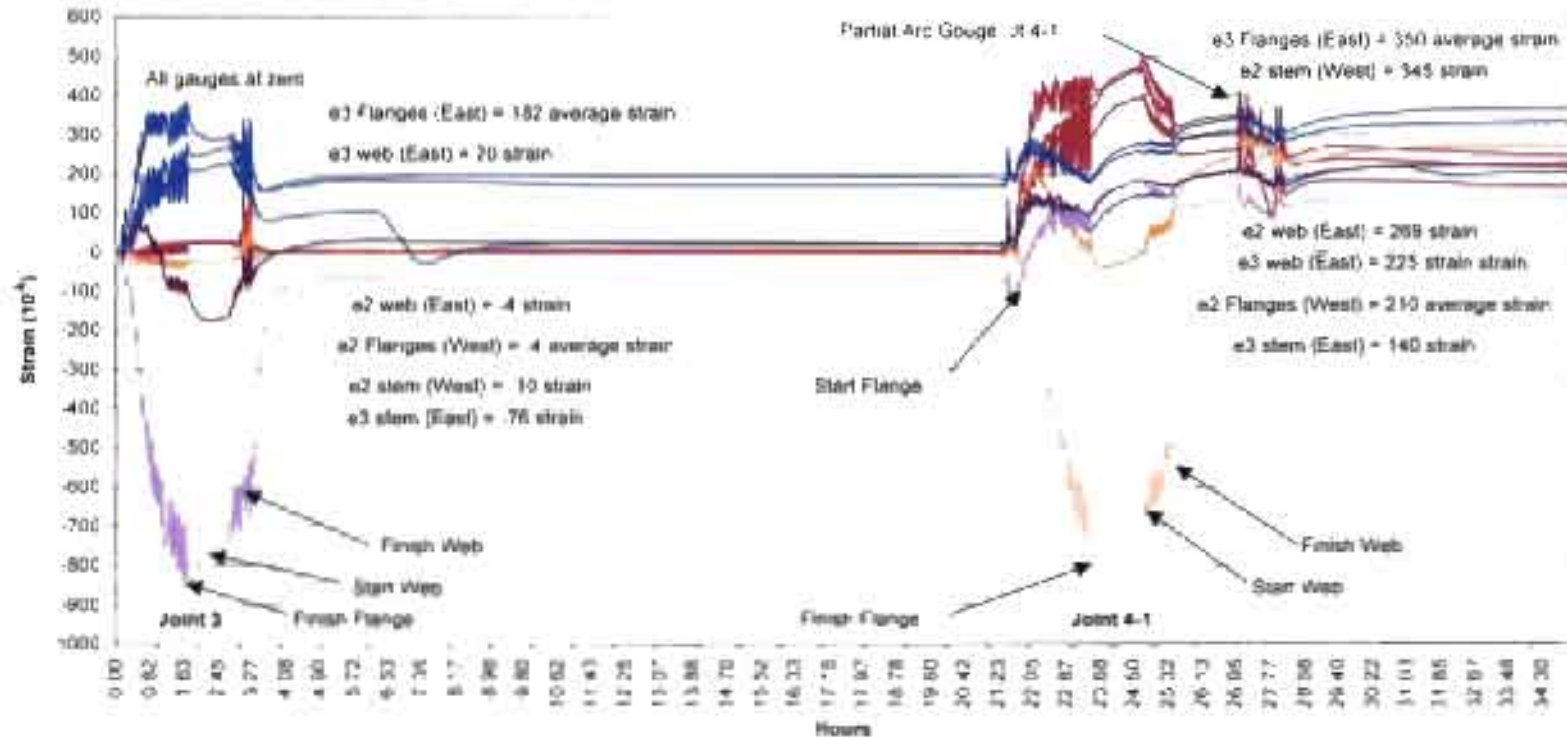


Figure 15. Graph - Strain Versus Time, WT-3, Joints 3 & 4-1

**Strain versus Time,  
WT-3, Joint 4-2, Detail, Stations 2 (West) and 3 (East), less SG e2M**

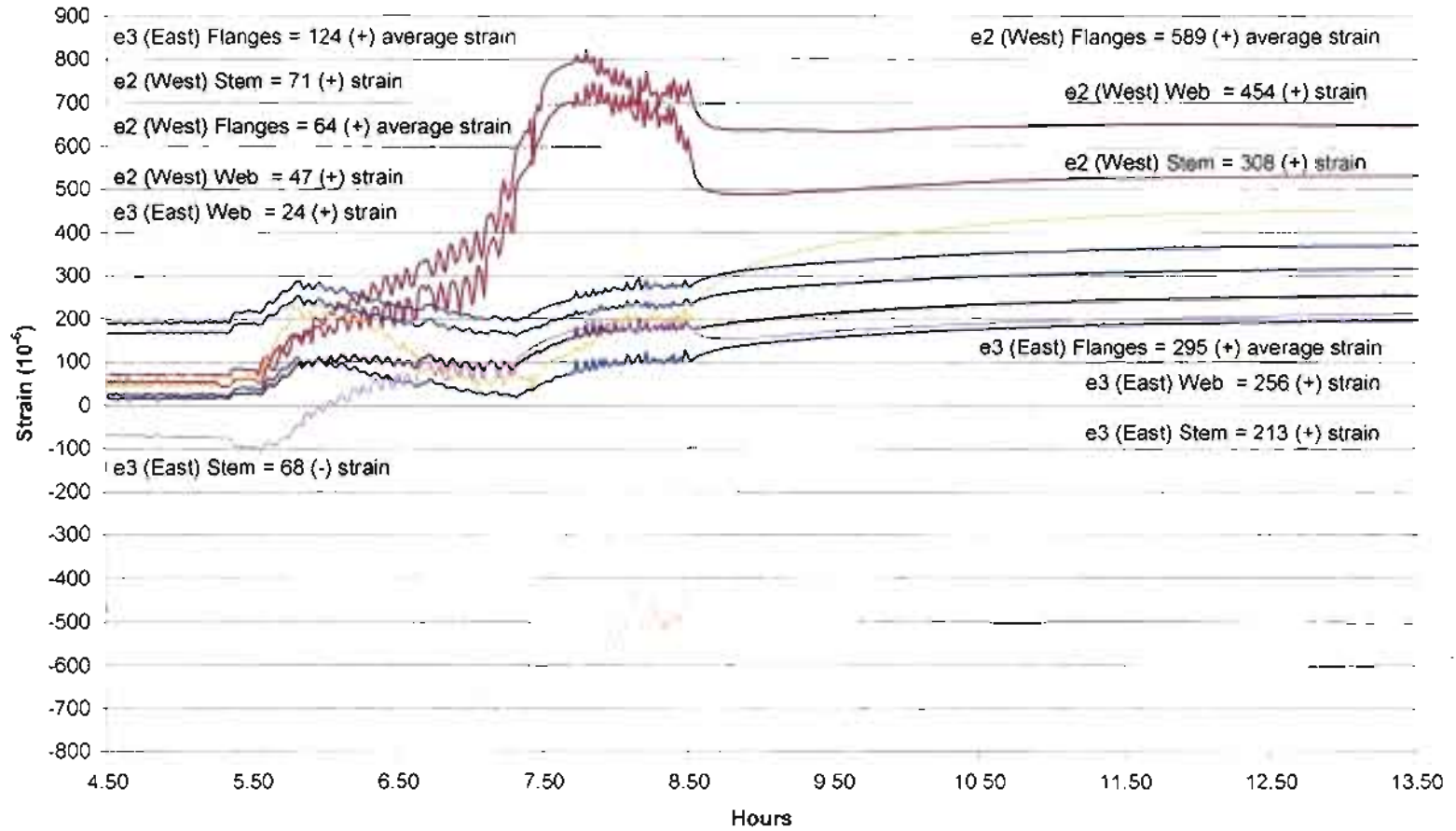


Figure 16. Graph - Strain Versus Time, WT-3, Joint 4-2

### Displacement versus Time WT-1, Joints 1 & 2

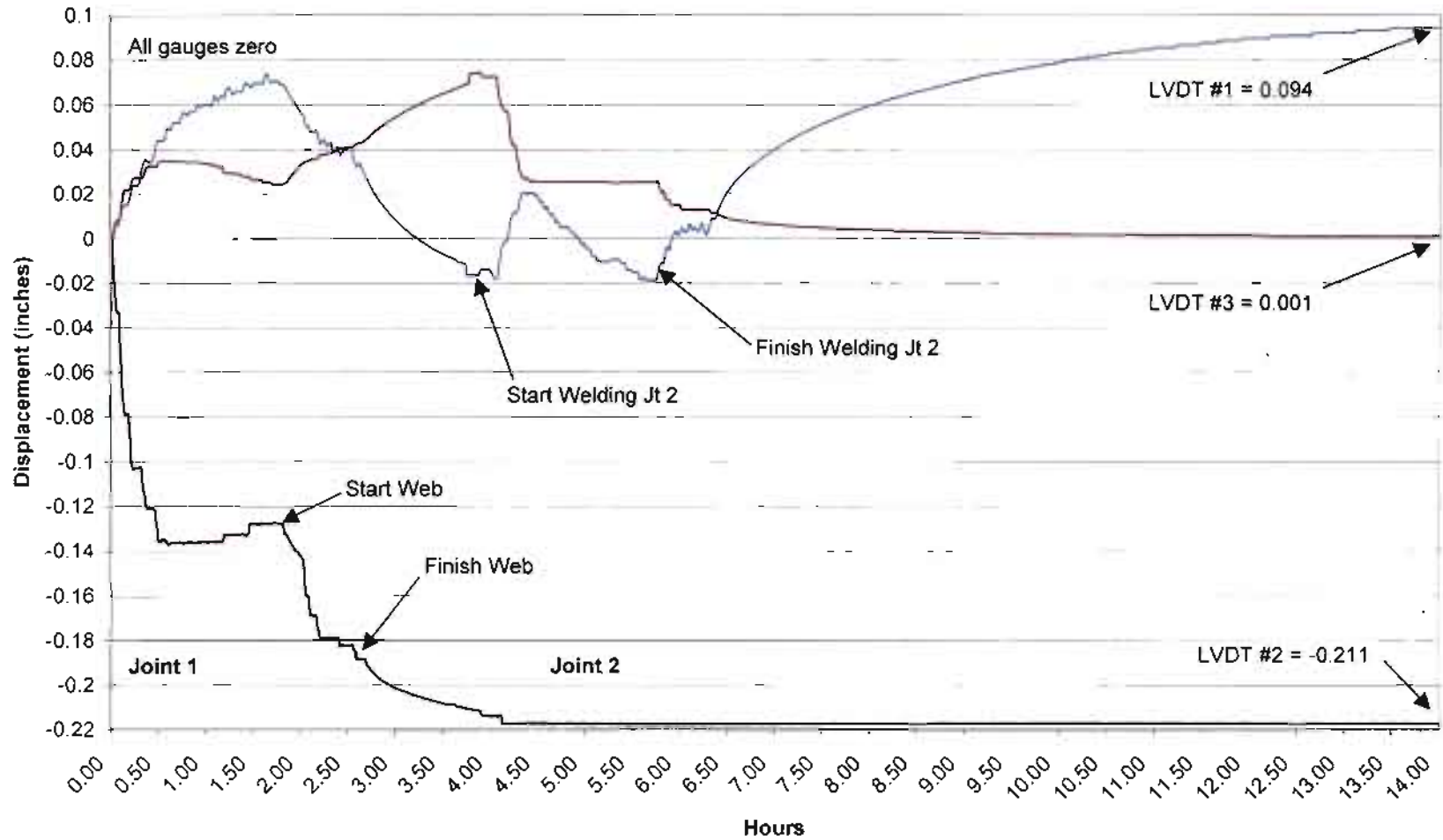


Figure 17. Graph - Displacement Versus Time, WT-1, Joints 1 & 2



Displacement versus Time  
WT-2 Joints 3 & 4-1

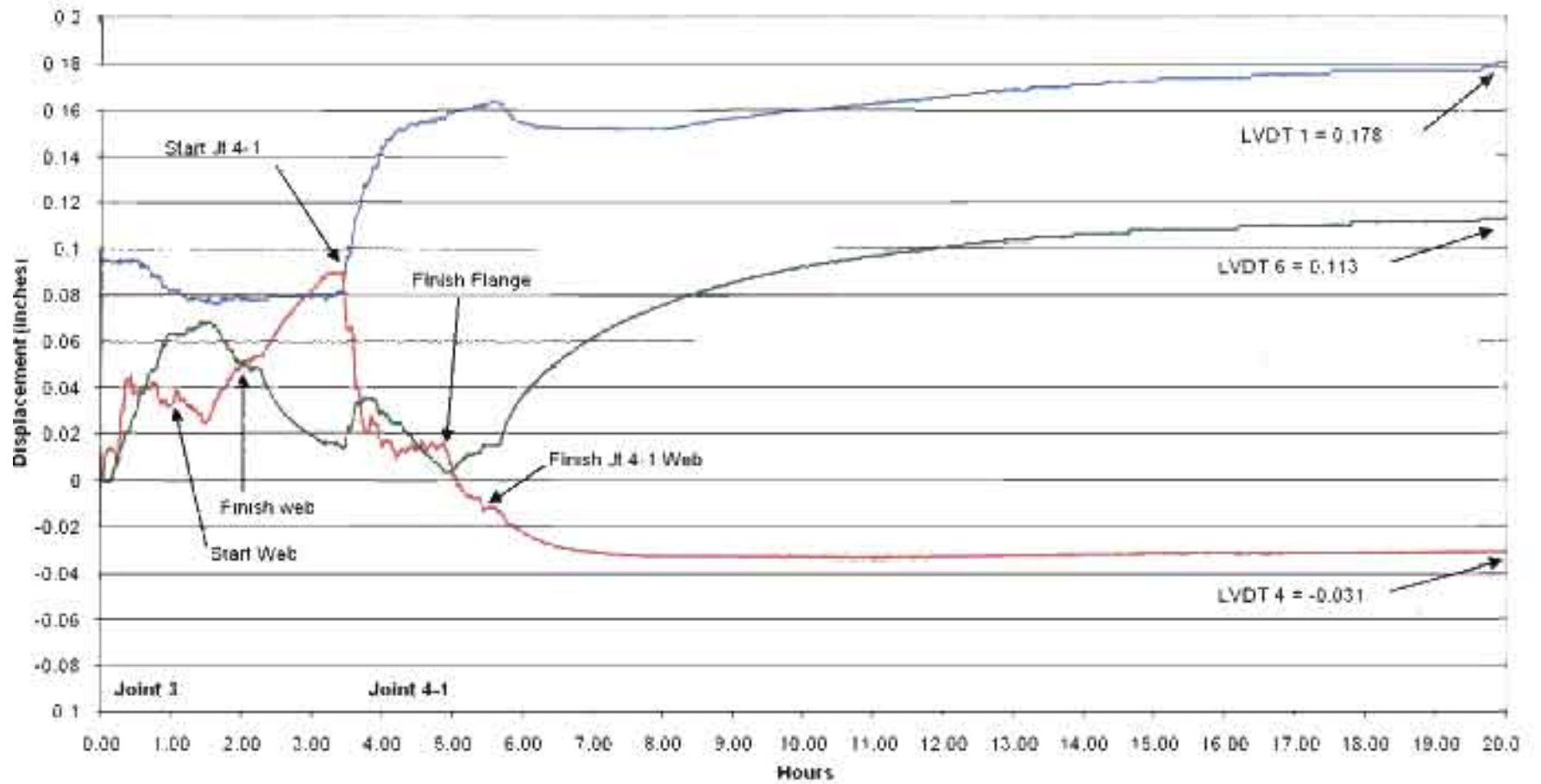


Figure 18. Graph - Displacement Versus Time, WT-2, Joint 3 & 4-1

Displacement versus Time,  
WT-3, Joints 3 & 4-1

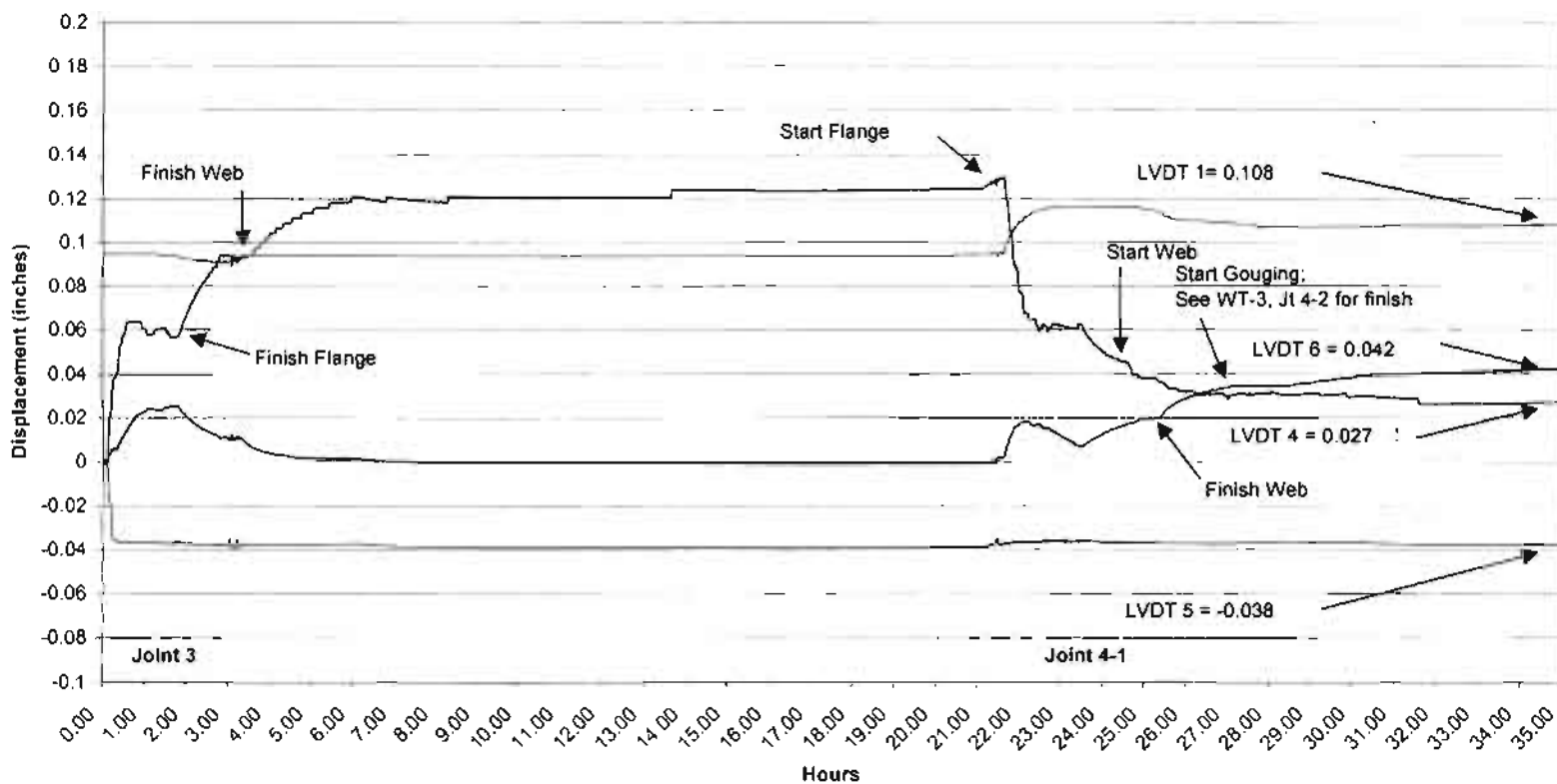


Figure 19. Graph - Displacement Versus Time, WT-3, Joints 3 & 4-1

Displacement versus Time.  
WT-3. Joint 4-2. with Removal of Weld 4-1

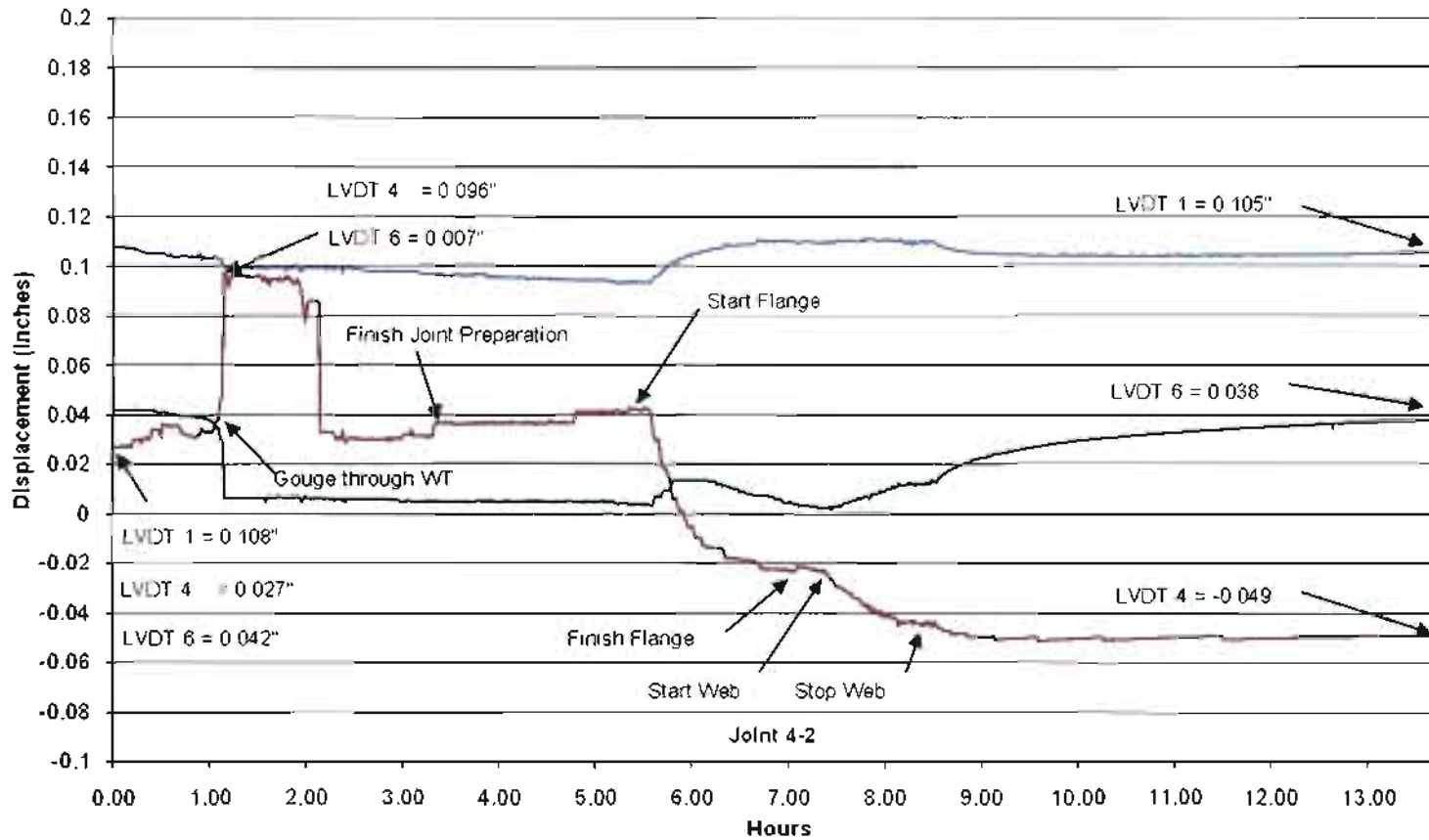


Figure 20. Graph - Displacement Versus Time, WT-3, Joint 4-1 Removal and Joint 4-2

### 3.2. Analyzing Strain Gradients

The strain graphs characterize the effects of increasing restraint upon the structural frame. Initially the beam is under no strain bolted into the test fixture. During the first 30 minutes of welding, each graph shows weld layers increasingly lock up the joint and strain increases rapidly. The initial weld layers cool to Region L<sub>2</sub> temperatures and become strong enough to restrain the joint from further contraction. Strains rapidly increase as the joint fills and restraint increases.

Table 3 summarizes the strain remaining in the frame after welding each joint. The data are sorted for restraint condition. Joints 1 and 3 under medium restraint are at the top of the table and Joints 2 and 4 under high restraint are at the bottom. These results are combined in the table to facilitate comparison of the residual strain associated with different joint restraint levels. Table 4 is the same table with the strain compiled into resultant stress using Equation 2 for ease of reference.

WT-2, Joint 4-1, was welded before Joint 3 had reached equilibrium. Joint 3 was fully displaced toward the closing joint from residual thermal displacement. Free displacement of the joint to its equilibrium position at ambient temperature was restrained during this experiment in the series. The data are shaded to identify the deviation from experiment protocol. Restrained thermal displacement at Joint 3 was superimposed on the stress expected while welding Joint 4-1. As Joint 3 cooled, it released thermal displacement and put the stem of closing weld, Joint 4-1, in high compression. The highly restrained, closing weld is in uniform tension at ambient temperature when the previous medium-restrained joint is at equilibrium before welding.

Table 3. Resultant Residual Strain

WT	Joint	$\epsilon_1$			$\epsilon_2$			$\epsilon_3$		
		Flg AVE	Web	Stem	Flg AVE	Web	Stem	Flg AVE	Web	Stem
1	1	62	-3	-119	N/A	N/A	N/A	N/A	N/A	N/A
2	3	Not At Equilibrium			N/A	N/A	N/A	N/A	N/A	N/A
3	3	6	6	10	-4	-4	-10	182	20	-76
4	3	-2	0	-1	9	-56	-66	104	-72	-503
1	2	215	138	32	N/A	N/A	N/A	N/A	N/A	N/A
2	4-1	-28	38	146	363	130	-305	428	-43	-74
3	4-1	88	95	98	210	269	345	350	225	140
3	4-2	96	97	99	589	454	308	295	256	213

Table 4. Resultant Residual Stress

WT	Joint	$\epsilon_1$			$\epsilon_2$			$\epsilon_3$		
		Flg AVE MPa (ksi)	Web MPa (ksi)	Stem MPa (ksi)	Flg AVE MPa (ksi)	Web MPa (ksi)	Stem MPa (ksi)	Flg AVE MPa (ksi)	Web MPa (ksi)	Stem MPa (ksi)
1	1	14.7 (2.1)	-0.7 (-0.1)	-28.3 (-4.1)	N/A	N/A	N/A	N/A	N/A	N/A
2	3	Not At Equilibrium			N/A	N/A	N/A	N/A	N/A	N/A
3	3	1.4 (0.2)	1.4 (0.2)	2.4 (0.3)	-1.0 (-0.1)	-1.0 (-0.1)	-2.4 (-0.3)	43.3 (6.3)	4.8 (0.7)	-18.1 (-2.6)
4	3	-0.5 (-0.1)	0	-0.2 (-0.03)	2.1 (0.3)	-13.3 (-1.9)	-15.7 (-2.3)	24.7 (3.6)	-17.1 (-2.5)	-119.6 (-17.3)
1	2	51 (7.4)	32.8 (4.8)	7.6 (1.1)	N/A	N/A	N/A	N/A	N/A	N/A
2	4-1	-6.7 (-1.0)	9.0 (1.3)	34.7 (5.0)	86.3 (12.5)	30.9 (4.5)	-72.5 (-10.5)	101.8 (14.8)	-10.2 (-1.5)	-17.6 (2.6)
3	4-1	20.9 (3.0)	22.6 (3.3)	23.3 (3.4)	49.9 (7.2)	64.0 (9.3)	82.0 (11.9)	83.2 (12.1)	53.5 (7.8)	33.3 (4.8)
3	4-2	22.8 (3.3)	23.0 (3.3)	23.5 (3.4)	140.0 (20.3)	107.9 (15.7)	73.2 (10.6)	70.1 (10.2)	60.9 (8.8)	50.6 (7.3)

Welding the highly-restrained, closing joint before the thermal displacement in the far-end, medium-restrained connection is released is a common assembly sequence when welding trusses. Welders weld all of the connections in a truss bay or work area before moving equipment along the structure. This assembly sequence used in WT-2 has the second highest residual strain in the frame, adding 82 MPa (12 ksi) of tension to the frame at the flange of the medium-restraint Joint 3, and the highest compression at 62

MPa (9 ksi) in the stem of the closing weld, Joint 4-1. The ultimate magnitude of welding strain is similar throughout the series of experiments.

The data collection for WT-2, Joint 4-2, was stopped prematurely and strain data at equilibrium were lost. And the data obtained from the closing weld in WT-3, Joint 4-1 did not appear as expected. The final strain gradients of this experiment indicated the welded closing flange was at the second lowest tension in the system while the web stem was the second highest, opposite of all other experiments. The flanges, with their greater weld area, should be in greater tension than the web stem. This anomaly is explained by the experiment methodology. The methodology specifies removing Joint 4-1 by the air-carbon arc cutting process and rewelding it as Joint 4-2. In this experiment, the cutting process was interrupted before the joint was completely cut out of the frame. Approximately three-quarters of the flange was gouged out of the joint before work was stopped for the day. The joint continued to cool to equilibrium, but the centroid of the connection had dropped into the web of the WT beam. The web weld increasingly carried residual tension in the structural frame. The data are shaded to identify the deviation from experiment protocol.

The strain data identify a force-couple that develops while welding the thick joint. The web goes into compression while the flange is welded because of the pinning reaction at the erection bolts. The flange and stem strain arcs reach their respective maxima and minima just before beginning to weld the web. Welding the web pulls the WT beam around the flange weld to reduce the tension in the flange. The slug of colder weld metal acts like a hinge that pins the joint but permits rotation. More weld metal is laid into the flange overall than in the web, however, and the web weld will not

completely eliminate the flange strain. The strain graphs confirm that considerable strain is relieved after welding is completed. Free displacement of the connection reduces residual stress.

Stresses from welding the fixed-end, high-restraint joint are translated to the West Bay beam-to-column assembly by the reaction with the structural frame. All of the strain gauges at West Bay Station 1 undergo a 10-fold increase in tension with each closing weld. The highly restrained closing weld changes the strain distribution so the entire frame is in tension.

Comparing the strain data in Table 3, two characteristics are observed that define medium and high joint restraint. First, welding strains under medium restraint are approximately half of the strains observed under high restraint. The highest strain imposed by welding a medium restrained joint occurred while welding WT-3, Joint 3. The stress this strain created was approximately 34.5 MPa (5 ksi) tensile. This is 38% less than the lowest flange tension recorded during high restraint and 69% less than the highest flange tension. Without global structural restraint, medium restrained joints hold less residual welding strain than highly restrained joints.

Second, given a structural geometry that can react to the shrinking connection, the strain distribution between medium and highly restrained joints in the test fixture is different. The strain in the medium-restraint joint goes from tensile in the flange to compression in the stem. Triaxiality cannot develop in these connections because the compressive stress relieves the structural potential for plane-strain stress. There is always some region of compression in the connection under medium restraint. Compression permits shear stresses to build in the connection to promote ductile yielding.

Both ends of the WT are under tension after the high-restraint, closing weld is finished. While welding the medium-restrained joint of WT-3, the compiled data at Strain Gage 3 show residual tension stress in Joint 3, climbed from 29 MPa to 70 MPa (4.2 ksi to 10 ksi) after the closing Joint 4 was welded. The data from Strain Gage 2 at the closing joint indicate the high-restraint WT-3, Joint 4-2, retained the greatest residual strains in the test fixture. The flange at Joint 4-2, under the welding arc, stabilized at 140 MPa (20 ksi) tensile stress. The least strain in WT-3 was observed at the stem of Joint 3 and it added 33 MPa (4.8 ksi) to the preload on the frame. All connections in highly restrained structures are under tension after welding. Because all welds are under tensile strain, triaxiality builds, robbing the connection of its expected ductility.

### 3.3. Analysis of the LVDT Data for Joints Under Medium Restraint

Medium joint restraint results in a connection under high weld shrinking strains and low global strain. The restraint that builds in Regions  $L_3$  and  $L_2$  of the connection and the reduction of thermal displacement are apparent in the LVDT data. LVDT 3 and 4 measure the expanding welding gap at the free end of the WT beams. As long as this gap expands, the welding stress is being relieved by displacement.

All of the welds initially exhibited a high rate of displacement, followed by a plateau after the initial weld layers lock the joint. The greatest rate of displacement occurs during the first 30 minutes of welding the flange. These weld layers cool to Region  $L_2$  temperatures. They resist the shrinking of the molten metal above them, creating medium restraint in the joint. Displacement is the result of the thermal energy introduced in Region  $L_3$  by welding and preheat introduced in Region  $L_2$ . The shrinking flange weld displaced between 0.9 – 1.7 mm (0.035 – 0.065 in) in the first 30 minutes.



The flanges took approximately 1.5 to 2 hours to completely weld out. No further displacement took place after 30 minutes until the beam web welding began. It took approximately 0.5 – 0.75 hours to completely weld out the webs. The free-end gap at Joint 4 increased again while the web was welded.

The initial solidified weld layers appear to act like a hinge as additional weld layers in the flange shrink and pull the WT. The erection bolts at the free-end of the WT restrain the beam from rotating into the shrinking flange weld. The force-couple that forms between the shrinking flange weld and the resisting bolts, identified by the strain data in 3.2, is reduced by WT web-to-column flange weld. The shrinking web pulls against the hinge-like flange weld, reducing residual stress in the joint and reduces the rotation against the free-end erection bolts. The web welds are readily observed in the LVDT data. These welds, cooling from Region L<sub>3</sub> heating, shrink and increase the overall displacement at the free-end LVDT.

The frame continued to displace after welding the medium-restraint Joints 1 and 3. LVDT 4 at the free-end recorded expansion after welding. This is because the medium-restraint connection, now completely fixed into the beam-to-column assembly, acts as one piece. The column flange adjacent to the weld expanded during welding from the thermal Region L<sub>2</sub>, heated between 66 to 260°C (150 to 500° F). The expanded flange temporarily bends the column into welding heat. As it cools, the column straightens out as the heated column flange shrinks back to its original length at ambient temperature. The WT, now completely welded into the column flange, follows the displacing column and expands the free-end weld gap at Joint 4.

In experiment WT-3, LVDT 4 and LVDT 5 were attached to the same point on

the WT beam to oppose each other. The displacement after welding described in Figure 19 is a result of the thermal effects in Region L<sub>2</sub>. LVDT 4 measured displacement at the free end of the WT beam. LVDT 5 measured displacement at Joint 3 directly under the welded joint and adjacent column. In the first 30 minutes, the LVDT displaced at the same rate and in opposite directions. The joint under the welding arc shrank and the free-end gap expanded. Once the weld at Joint 3 was completed, LVDT 5 stopped displacing. LVDT 4, however, continued to displace hours after welding was completed. The thermal displacement from residual heat in the joint was very consistent over four welding sequences. The cooling column caused the free-end gap to expand displacing 2 mm (0.079 in) in all but one weld. Table 5 details the displacement data of LVDT 3 and 4.

LVDT 1 and 6 are attached at the exterior columns of the experiment assembly and the stationary structural frame. They measure the bending test fixture reacting against the Region L<sub>3</sub> and L<sub>2</sub> displacements. These columns, away from the high-restraint, closing welds, are at ambient temperatures and characterize Region L<sub>1</sub> in the thermal system. LVDT 1 and 6 extend as the columns bend under the heat while welding the medium-restraint connections and retract as the column flange cools. Column displacement virtually returns to zero in WT-3 and WT-4. Other than the free-end erection bolts pinning the WT beam from rotation, the test fixture imposes no further restraint or added residual strain to the connection. Table 6 details the displacement data of LVDT 1 and 6. LVDT 1 has a permanent positive displacement because Joint 2 was welded before Joint 1 reached equilibrium, pinning the thermal displacement into the West column.

Table 5. Displacement Data Detail ~ Medium Restraint, Far Column

WT	Weld		Initial	Finish Weld	Thermal	Overall	Weld
	Joint	LVDT	Displacement mm (in)	Displacement mm (in)	Displacement mm (in)	Displacement mm (in)	Area cm <sup>2</sup> (in <sup>2</sup> )
1	1	3	0.000	1.1 (0.043)	0.79 (0.031)	1.9 (0.074)	15.7 (2.43)
2	3	4	0.000	1.3 (0.053)	0.93 (0.037)	2.3 (0.090)	16.6 (2.57)
3	3	4	0.000	2.4 (0.093)	0.79 (0.031)	3.1 (0.124)	17.0 (2.63)
4	3	4	-0.2 (-0.008)	1.3 (0.052)	0.79 (0.031)	2.1 (0.083)	16.6 (2.57)

Table 6. Displacement Data Detail ~ Medium Restraint, Adjacent Column

WT	Weld		Initial	Finish Weld	Thermal	Overall
	Joint	LVDT	Displacement mm (in)	Displacement mm (in)	Displacement mm (in)	Displacement mm (in)
1	1	1	0.000	0.81 (0.032)	-1.2 (-0.049)	-0.4 (-0.017)
2	3	6	0.000	1.2 (0.048)	-0.8 (-0.033)	0.4 (0.015)
3	3	6	0.000	0.3 (0.011)	-0.3 (-0.012)	0.03 (-0.001)
4	3	6	0.13 (0.005)	0.2 (0.009)	-0.2 (-0.006)	-0.05 (-0.002)

### 3.4. Analysis of the LVDT Data for Highly Restrained Joints

The displacement of the highly restrained connections displayed in the LVDT data is similar to the displacement exhibited by the connections under medium restraint. The weld at the closing joint shrinks, causing the LVDT under the joint to retract. The horizontal beam is no longer free to slide along the x-axis because the welded column resists all displacement in Regions L<sub>3</sub> and L<sub>2</sub>. The room temperature test fixture adds global Region L<sub>1</sub> restraint to the connection, far from the thermal energy created by the electric arc. The far columns act to resist maximum potential displacement of the column flanges. The beam flanges and adjacent column, however, displace upward and inward.

Unlike joints under medium restraint, this joint displacement is achieved at the expense of the columns. The cooling weld zone and the regional thermal displacement pull the columns out of plane when the weldments finally reach equilibrium. Joints 2, 4-1, and 4-2 in LVDT displacement graphs graphically characterize the displacement of highly restrained connections from the thermal energy of the welding arc. Table 7 summarizes the data for LVDT 3 and 4 underneath the highly restrained closing joints. LVDT 4 failed while welding WT-2 and Joint 4-2 data were unavailable. The large difference in overall displacement observed while welding WT- 1 and WT-2 occurred because the frame was not at equilibrium before welding the closing welds. For WT-3, weld shrinking and thermal displacement were similar during all stages of the welding cycle. For high-restraint joints, the displacement from welding shrinking was never less than three times greater than the thermal displacement and as much as seven times greater in experiments for WT-2. These data conflict with the observations made by Masubushi et al. (1987) where thermal displacement was greater than displacement from weld shrinking. Overall thermal displacement through the joint varied less than 0.8 mm (0.030 in) in five experiments. While overall displacement is similar between medium and high-restraint joints, Table 5 data identify twice as much thermal displacement in joints under medium restraint and less weld shrinking displacement. The weld metal stretches more under high restraint. The data in Table 7 summarize the displacement of LVDT 1 and 6 at the exterior columns fixing the ends of the highly restrained beam. The data in Table 8 illustrate the correlation between increasing joint restraint and increased residual weld stress in the structural system.

The columns are at full material strength and their orientation in the frame offers

Table 7. Displacement Data Detail - High Restraint, Adjacent Column

Weld			Initial	Finish Weld	Thermal	Overall	Weld Area
WT	Joint	LVDT	Displacement	Displacement	Displacement	Displacement	cm <sup>2</sup> (in <sup>2</sup> )
			mm (in)	mm (in)	mm (in)	mm (in)	
1	2	3	1.9 (0.074)	-1.4 (-0.056)	-0.4 (-0.017)	-1.9 (-0.073)	17.4 (2.71)
2	4-1	4	2.3 (0.090)	-2.6 (-0.103)	-0.5 (-0.018)	-3.1 (-0.121)	14.7 (2.28)
2	4-2	4	NG	NG	NG	NG	18.5 (2.87)
3	4-1	4	3.1 (0.124)	-2.2 (-0.086)	-0.3 (-0.011)	-2.5 (-0.097)	19.9 (3.08)
3	4-2	4	1.4 (0.054)	-2.2 (-0.087)	-0.1 (-0.005)	-2.3 (-0.092)	23.2 (3.60)

Table 8. Displacement Data Detail ~ High Restraint, Far Column

WT	Weld Joint	LVDT	Initial Displacement	Finish Weld Displacement	Thermal Displacement	Overall Displacement
			mm (in)	mm (in)	mm (in)	mm (in)
1	2	1	-0.4 (-0.017)	0.6 (0.024)	2.6 (0.101)	2.8 (0.111)
2	4-1	6	0.4 (0.015)	0.0	2.5 (0.098)	2.5 (0.098)
2	4-2	6	1.8 (0.071)	0.2 (0.006)	NG	NG
3	4-1	6	-0.02 (-0.001)	0.5 (0.020)	0.6 (0.023)	1.1 (0.043)
3	4-2	6	-0.5 (-0.019)	0.2 (0.009)	0.6 (0.025)	0.9 (0.034)
2	4-1	1	2.1 (0.082)	2.1 (0.082)	0.4 (0.014)	2.4 (0.096)
2	4-2	1	3.3 (.128)	1.6 (0.064)	NG	NG
3	4-1	1	2.4 (.093)	0.6 (0.023)	-0.2 (-0.008)	0.4 (0.015)
3	4-2	1	2.6 (0.101)	0.4 (0.016)	-0.1 (-0.004)	2.9 (0.113)

the greatest stiffness and resistance to displacement. LVDT 1 and 6 show the stresses exerted by the shrinking weld in Region L<sub>3</sub> and the expanding adjacent flanges in Region L<sub>2</sub> are sufficient to bend the room-temperature columns out of plane, since no heat is applied to them. Regional displacement at the flange bends the interior column into the welds at joints 4-1 and 4-2. The column pushes the WT beam against the East exterior column at LVDT 6 and pulls against the West Bay frame at LVDT 1. After the flange is welded and welding of the web is started, LVDT 6 changes direction and begins to

increase in length. The maximum thermal displacement of the interior column flange and the shrinking web weld pull on the exterior column. As the interior column flange cools, it attempts to straighten to its original position. LVDT 6 continues to increase in length rapidly for over 2 hours after welding is completed and continues to displace for hours.

LVDT 1 compliments the pattern of LVDT 6 while Joint 2 is welded. It does not decrease in length after welding is completed, however. This apparent anomaly occurred because the Weld 2 was made without allowing Joint 1 to reach equilibrium. The West Bay was welded into an hourglass shape. Data collection was halted before the connection reached equilibrium during WT-2, Joint 4-2. Thermal and overall LVDT displacement could not be evaluated.

The residual heat in the connection combines with the heat of the welding arc to make the adjacent column flange and connecting beam expand. The rest of the structural test fixture resists the regional expansion at the welded flange. A force-couple is temporarily induced in the beam-to-column connection adjacent to the welding arc by the regional thermal expansion. This is not the force-couple observed in the shrinking weld around the centroid of the connection described in 3.2. The flanges expand and bow around the cold steel into the weld. It is the expanding hot metal forcing displacement of the structural members. The force-couple that results from the global resistance to thermal expansion and weld contraction is welded into the frame. Medium-restraint connections return to their original positions at equilibrium and the weld root gap at the far-end joint increases. In highly restrained connections, thermal expansion bows the column into the weld, pulling the columns out of plane and fixing the connection in a bowed, hourglass condition. The force-couple that results from global structural

resistance to thermal expansion and weld contraction is locked into the frame, increasing the residual stress in the structural frame.

### 3.5. Calculating the Resultant Stress

WT-2 and WT-3 beams were cut out of the East bay during the experiments. Joint 4 was cut through twice for each WT. Measurements were taken while three of these cuts were made. The cut, or kerf, was observed to spring open in all cases. Residual tensile welding stress in the test fixture drove this immediate and noticeable expansion.

Figure 20 and Figure 21 display LVDT data that show the sudden release of tension. The displacement is most obvious in LVDT 4 immediately under the joint. It lengthens when the last joint ligament is cut through. LVDT 1 and 6 at the exterior columns immediately shorten as they snap to their original position before welding pulled them out of plane. LVDT 1, measuring the translation to the West Bay, moves less than LVDT 6 at the single column in the East Bay. The two columns in the West Bay resist the pull of the weld.

The strain gauge data displayed in Figure 22 and Figure 23 show the release of tension in the structural frame, too. The thick flange was cut through first, and then the web. The strain gradients show the strain gradually being shed by the thinning flange weld, and picked up by the remaining web weld. The strain gauge data at Station 2 near the cut best describe the release of tension in the structural frame. The strain gauges at Stations 1 and 3 identified decreasing strain after the cuts were made. But they also measured strain in the frame from the other remaining welds and energy absorbed by elastic displacement of the remaining structural members. These graphs have not been presented here.

Displacement versus Time,  
WT-2, Jt 4-1 Removal

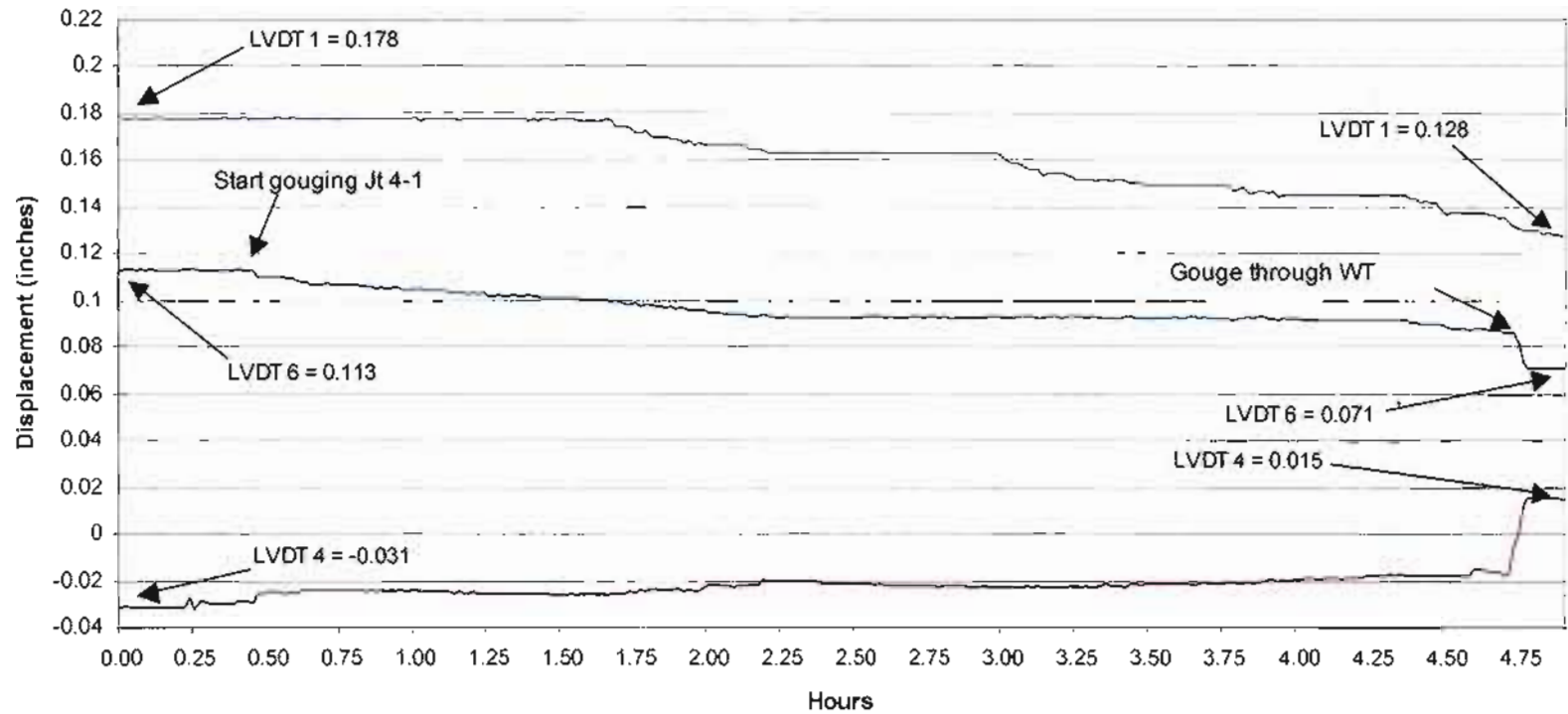


Figure 21. Displacement Versus Time, WT-2, Joint 4-1 Removal



**Strain versus Time,  
WT-2, Joint 4-1 Removal, Stations 2 & 3**

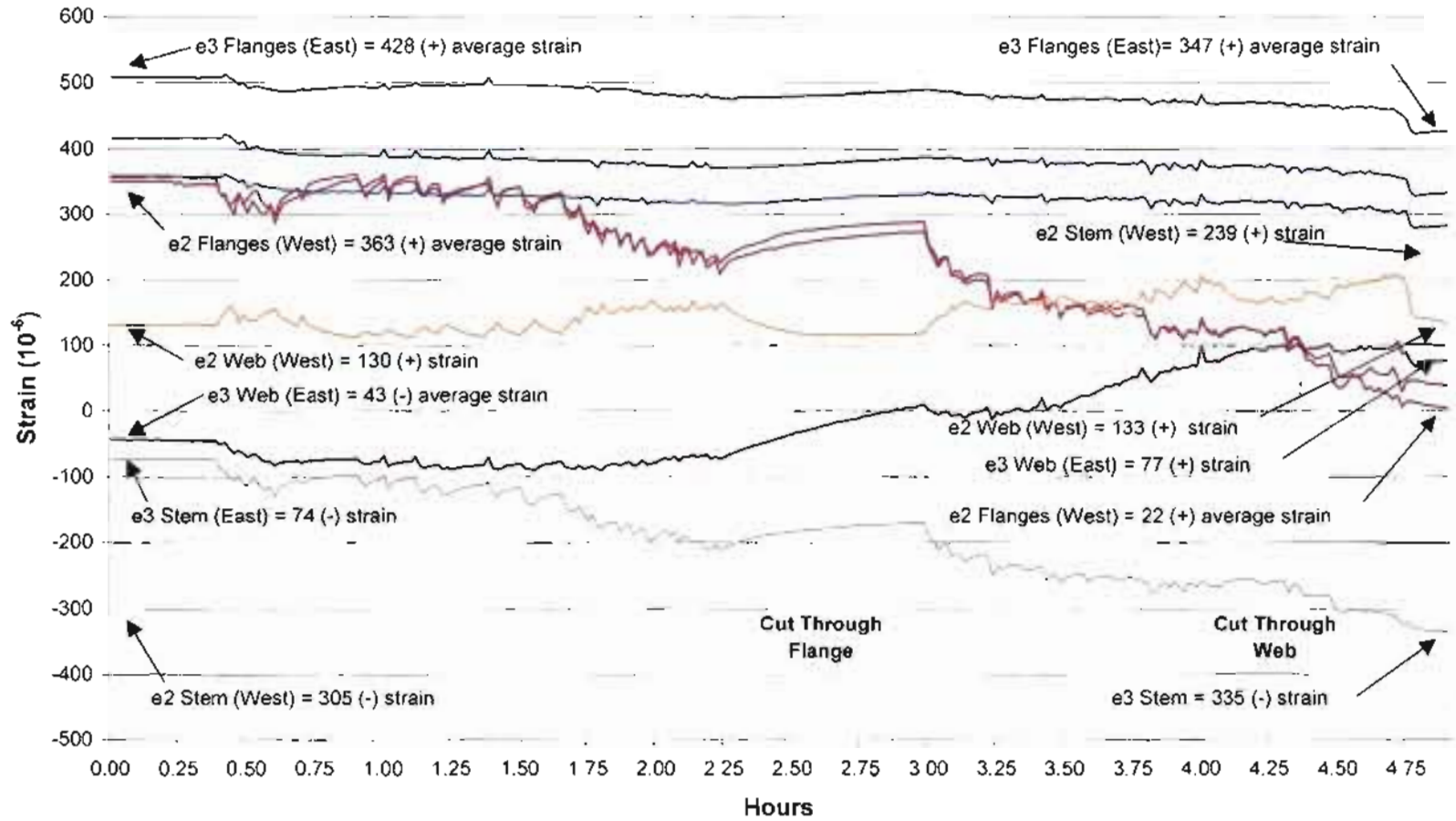


Figure 22. Graph - Strain Versus Time, WT-2, Joint 4-1, Removal

Strain versus Time,  
WT-3, Joint 4-1 Cut-out, Station 2 (West) Detail

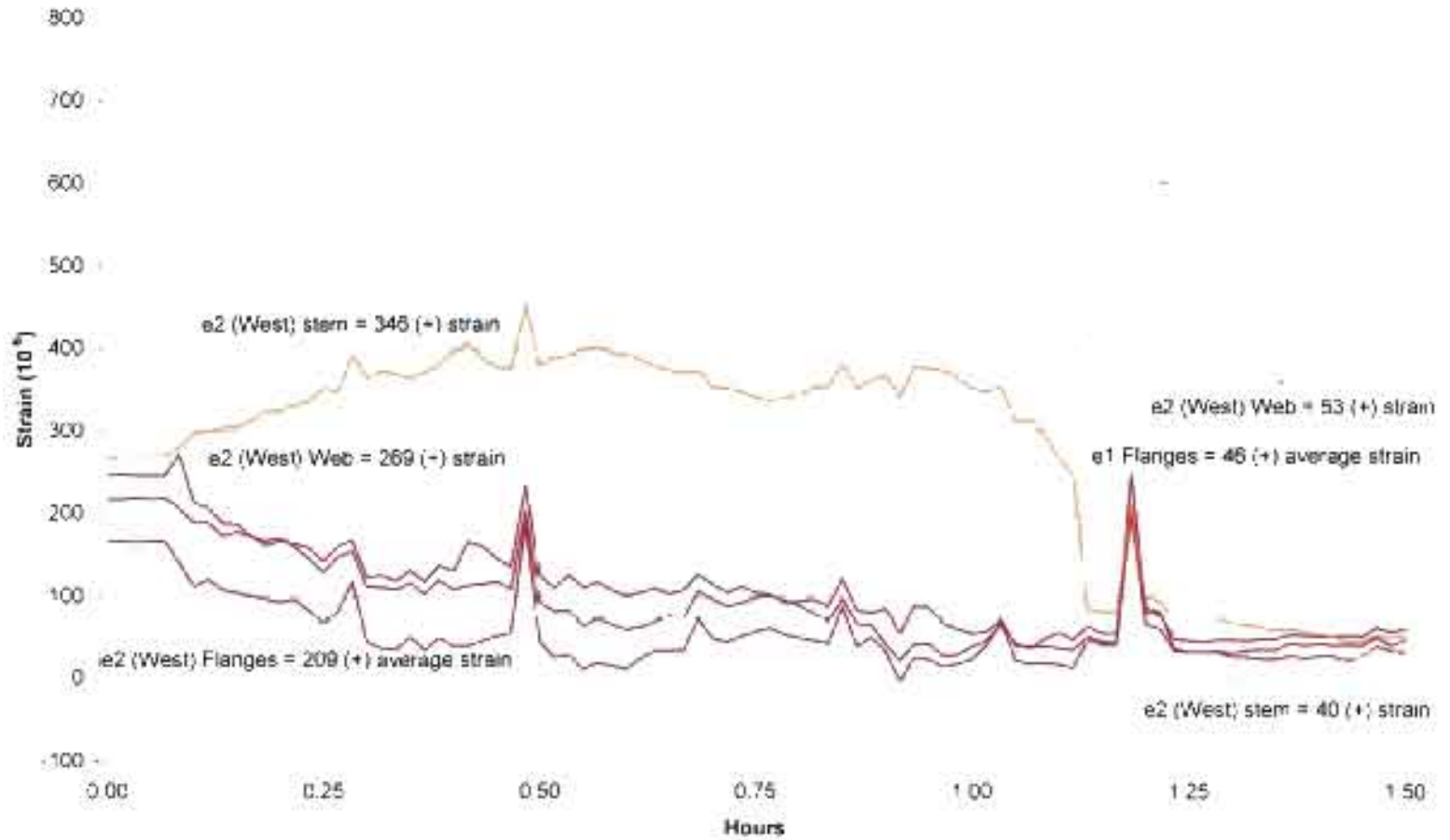


Figure 23. Graph - Strain Versus Time, WT-3, Joint 4-1, Removal

The magnitude of residual welding stress measured by the LVDT is calculated using Equation 10. The change in the LVDT length after cutting and the known material properties are entered into the formula. Equation 2, expanded for Young's Modulus of Elasticity from Equation 10, converts the change in strain into stress on the section area. The conversions are shown in Table 9 for the displacement data and Table 10 for the strain gauge data. The data indicate welding stresses are 33 to 51% of the designed yield strength of the structural frame.

Table 9. Change in Residual Stress – Displacement Gauges

WT	Weld Joint	LVDT	Displacement Before Cut mm (in)	Displacement After Cut mm (in)	Change in Length, $\Delta L$ mm (in)	Displacement Stress Loss MPa (ksi)
	4-1				1.2	
2	Removal	4	-0.8 (-0.031)	0.4 (0.015)	(0.046)	117 (16.9)
	4-1				1.8	
3	Removal	4	0.7 (0.027)	2.4 (0.096)	(0.069)	174 (25.3)

Table 10. Change in Residual Stress - Strain Gauges

WT	Weld Joint	Gauge Station	Strain Gauge	Strain Before Cut $\mu\epsilon$	Strain After Cut $\mu\epsilon$	Change in Strain $\mu\epsilon$	Displacement Stress Loss MPa (ksi)
	4-1						
2	Removal	2	Stem	-380	239	619	124 (18.0)
	4-1						
3	Removal	2	Stem	719	0	-719	-144 (-20.9)

The impact of welding WT-2, Joint 4-1, before Joint 3 had reached equilibrium is reflected in these data. A force-couple introduced into the frame discussed in Section 3.4

put the stem of WT-2, Joint 4-1, in compression. Even though the residual welding stress is tensile, the residual welding stress release appears negative. The LVDT data confirm the joint snapped open after gouging.

The experimental residual welding stress measured by the LVDT correlates well with the stress calculated using the strain gauge data. For WT-2 and WT-3, the calculated stress values for the LVDT and strain gauges deviate by less than 7% and 21% from one another, respectively. These results indicate that while the residual welding stress is sufficient to pull the large structural members out of plane, it does not approach the 345 MPa (50 ksi) minimum yield strength of the structural members nor the 400 MPa (58 ksi) minimum yield strength of the weld filler metal.

Actual residual welding stress measured during the experiment series is less than half of what is generally expected in the literature (Lincoln Electric (1994); Masubuchi et al. (1987)). These results are not surprising. As each weld bead is made, the heat from the welding arc tempers the previous bead. If the bead beneath the arc is raised to 538°C (1000°F), it retains little more than 50% of its yield strength at ambient temperatures (ASTM 1972). The weld must shed stress exceeding the high temperature yield strength through plastic displacement. The tempered bead will only retain the stress not shed plastically, or no more than 172 MPa (25 ksi). The thick weld connection undergoes many excursions between preheat temperature and 538°C (1000°F) before welding is complete. The connections in the present experiments typically hovered between 177°C and 249°C (350°F and 480°F) during welding. Material yield strength is reduced 15% at these temperatures and stress shedding will occur.

### 3.6. Joint Restraint and the AWS Displacement Equations

AWS joint displacement equations, Equation 5 and 6, suggest a direct relationship of overall joint displacement with the average weld area. The experimental data indicate joint displacement is dependent upon the relative joint restraint. Definitions of Medium and High joint restraint were established in detail in 2.1. The first weld in a moment frame, where the weld beads, themselves, restrain the joint from free movement illustrate a joint under medium restraint. The closing joint, welding against a beam totally fixed by welding to the far-end column while shrinking against a fixed frame illustrates a joint under high restraint. Table 11 compares the calculated results of the AWS equations with the experimental displacement data and the measured weld areas from Table 5 and Table 7 for the different restraint environments. Equation 5 was closest to predicting the magnitude of joint displacement. No equation described the displacement of the highly restrained connections well.

With one exception, the joint displacement of medium restrained joints increased as the weld area increased. Joint 3 of WT-4 had the same weld area as Joint 3 of WT-2, but displaced 0.2 mm (0.007 in) less. This is a very small amount of deviation in over thirty or more weld passes. Only Joint 3 of WT-3 matched Equation 5, the outdated first AWS equation. None of the actual data for medium restrained joints compared well with Equation 6, the current AWS displacement equation. One weld shrank more than expected. Most welds shrank less.

The AWS relationship of weld displacement to weld area is not observed in the highly restrained, fixed end connections of Joints 3 and 4. The deviation of actual displacement of highly restrained joints compared with Equation 5 calculations

Table 11. AWS Predicted Displacement Versus Actual Displacement

WT	Weld Joint	LVDT	Equation 5 AWS Equation 1 Displacement mm (in)	Equation 6 AWS Equation 2 Displacement mm (in)	Actual Overall Displacement mm (in)	Weld Area cm <sup>2</sup> (in <sup>2</sup> )	Deviation from Equation 5	Deviation from Equation 6
1	1	3	2.8 (0.11)	5.8 (0.23)	1.9 (0.074)	15.7 (2.43)	47%	205%
2	3	4	2.8 (0.11)	6.4 (0.25)	2.3 (0.090)	16.6 (2.57)	22%	178%
3	3	4	3.1 (0.12)	6.6 (0.26)	3.1 (0.124)	17.0 (2.63)	0%	113%
4	3	4	2.5 (0.10)	5.6 (0.22)	2.1 (0.083)	16.6 (2.57)	19%	167%
1	2	3	3.1 (0.12)	6.9 (0.27)	1.9 (0.073)	17.4 (2.71)	63%	263%
2	4-1	4	2.5 (0.10)	5.6 (0.22)	3.1 (0.121)	14.7 (2.28)	-19%	81%
3	4-1	4	3.6 (0.14)	7.9 (0.31)	2.5 (0.097)	19.9 (3.08)	44%	216%
3	4-2	4	4.1 (0.16)	9.4 (0.37)	2.3 (0.092)	23.2 (3.60)	78%	309%

was scattered. For WT-3 Joint 4-2, the connection with the largest area, displaced second to the least overall. The joint shrank approximately 5% less than the shop-prepared Joint 4-1. WT-2 Joint 4-1, the joint with the smallest area, displaced the most. While Joint 4-2 had a 15% greater weld area than Joint 4-1, the displacement while welding was only 1% more than Joint 4-1. It is important to note that the joint displacement of Joint 4-2 from thermal effects after welding was 55% less than Joint 4-1. The same welder welded these welds, but it is very likely that the welding technique changed when Joint 4-2 was welded. Stringer bead technique was used to weld the narrower groove of Joint 4-1. A slight weave technique was used to bridge the wider groove in Joint 4-2. Wider beads would lock up the weld early in the welding sequence.

The global restraint of the fixed-end and the resisting columns also contribute to

the deviation of the calculated displacement from the experimental data. WT-2, Joint 4-1 was welded before Joint 3 returned to equilibrium. That joint displaced 18% more than any another fixed-end weld after welding was completed. This is explained by the fact that Joint 3 of WT-2 was still expanded by Region L<sub>2</sub>, regional displacement created by residual welding heat and preheat. The bending of the column into the weld minimized the effect of global restraint on the closing weld at Joint 4-1.

### 3.7. Evaluation of a Long-Span Truss

The effects of welding sequence on a Long-Span truss can be analyzed using the method of virtual work. This energy analysis technique offers a means of predicting displacement at a point along the truss by analyzing the calculated load-path through the truss. Each weld joint shrinks a little when it is finished. The regional effect of weld shrinking displacement on other points in the truss can be calculated by applying a virtual unit load at the point of interest. Any point in the structure, however, can be calculated using Equation 9, as explained in 2.1.3.

The truss connections are analyzed using the method of joints to develop the load path through the welded truss connections. This paper analyzes the effects of displacement of Point H in Figure 24, at the center of the truss. The truss is deconstructed into its parts to observe the shrinking effects applied to the truss connections. The top and bottom chords are cut into segments to observe the load effects progressing through the truss. Because the truss is symmetrical about the centerline GH, Figure 24 identifies the pieces in one-half of the truss assembly only. These piece marks identify the structural members in the virtual work calculations. A theoretical vertical point load is applied to the truss to calculate the reaction forces supporting the truss. With the forces in one

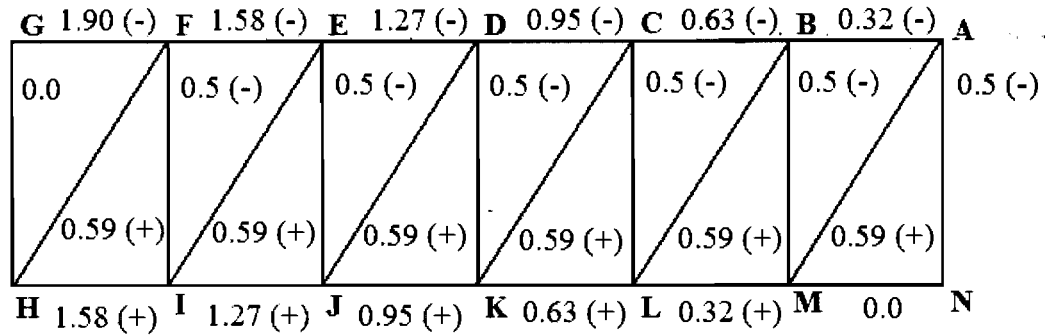


Figure 24. Analysis of a Truss at Point H

plane defined, the load path through the welded truss connections is calculated.

There are 14 connections in the long-span truss, disregarding the chord splices. They are shown in Figure 25. The web member GH, at the center of the truss, is a zero-force member. The axial load passes through the chords and diagonals into the adjoining bay with no transverse load path. The extension of the bottom chord joining the column, MN, is also a zero force member. Only three joint variations need analysis. Connections #1, #2, and #3 are analyzed in free body diagrams for a virtual unit load applied at Point H. Connection #1 differs from #2 or #3 because it is at the column.

Connections #1 and #3 show that as a vertical down unit point load,  $n$ , is applied to the bottom chord at Point H, the top chord goes into compression throughout its length. Compression forces increase out from the column in each bay until the middle of the truss is reached. Conversely, the bottom chord is in tension. Tension forces also increase along the truss to the center. The forces in the diagonal and web members remain constant throughout the truss relative to the applied forces imposed on the structure. The relative magnitude of the force effects and the direction of loading are implied by the free body diagrams.



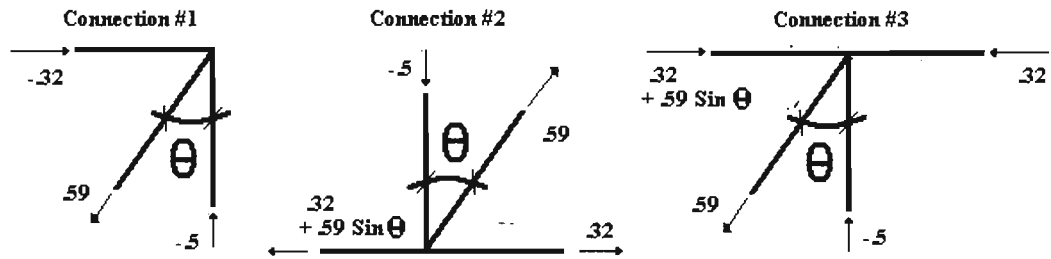


Figure 25. Truss Connection Free-Body Diagrams

The displacement data from Table 7 are entered into Equation 9 to predict the Point H displacement from residual welding stress. These data were taken directly under the welded joint. Because the residual tensile stress acts to shorten the member,  $\Delta L$  in Equation 9 is the joint displacement measured during these experiments. While welding WT-1 and WT-2, the closing joints shrank  $-1.9 \text{ mm}$  ( $-0.073 \text{ in}$ ) and  $-3.1 \text{ mm}$  ( $-0.121 \text{ in}$ ) respectively. These welds were started before the medium-restraint welds reached equilibrium. They illustrate a common welding sequence, discussed in 3.5, that resulted in 33% increase in overall displacement. Almost all of the thermal displacement remained locked into those frames. In Experiment WT-3, both of the shop and field closing weld configurations displace approximately  $-2.3 \text{ mm}$  ( $-0.09 \text{ in}$ ) after welding. The effects of residual welding stress on the truss are analyzed assuming a general displacement of  $-2.5 \text{ mm}$  ( $-0.10 \text{ in}$ ) in each joint welded.

If only one member shrinks during welding, that load is reflected with displacement at Point H. Table 12 illustrates the load effects applied by shrinking welds to Point H. The summation of all  $\Delta L$  displacement and force contribution of each member to vertical displacement at Point H gives the point's overall vertical displacement after welding. With no change in length, members drop out of the analysis.

Table 12 illustrates the effects when only one weld in each member CK and DK, and their complements on the opposite side of the truss, are made shorter by welding. Weld shrinking in four web members in the truss will cause Point H to displace 0.5 mm (0.02 in) downward. Should the weld sequence join the web members in a manner where all joints displace in a highly restrained condition without returning to equilibrium, the final vertical displacement at Point H will be 5.6 mm (0.22 in) downward. Adding a splice in the truss chords, in addition to the maximum welding displacement, will pull the final vertical displacement at Point H back up to 4.7 mm (0.18 in) down from its original position.

Table 12. Method of Virtual Work - Displacement at Point H

		$\Delta L$	N	$n\Delta L$
<b>Top Chord</b>	AB	0	-0.32	0
	BC	0	-0.63	0
	CD	0	-0.95	0
	DE	0	-1.27	0
	EF	0	-1.58	0
	FG	0	-1.9	0
	<b>Bottom Chord</b>	NM	0	0
ML		0	0.32	0
LK		0	0.63	0
KJ		0	0.95	0
JI		0	1.27	0
IH		0	1.58	0
<b>Diagonal</b>		AM	0	0.59
	BL	0	0.59	0
	CK	0.1	0.59	0.059
	DJ	0	0.59	0
	EI	0	0.59	0
	FH	0	0.59	0
	<b>Web</b>	AN	0	-0.5
BM		0	-0.5	0
CL		0	-0.5	0
DK		0.1	-0.5	-0.05
EJ		0	-0.5	0
FI		0	-0.5	0
GH		0	0	0
1/2 Vertical Displacement at H				0.009
<b>Total Vertical Displacement at H</b>				<b>0.018</b>

## 4. CONCLUSIONS

### 4.1. Characterization of Medium and High Joint Restraint

The full-scale experiments provided opportunities to observe the effects of restraint while welding ASTM Group 4 sections. The compiled data offer characteristics that describe conditions of medium and high joint restraint not provided in current literature. The data also call into question the limits of two commonly-held welding beliefs. Displacement through the welding joint is much less than predicted and the resulting residual stresses are not as high as generally assumed. Residual tensile stress from welding, however, is significant and prestresses the connection. The tension that remains after welding establishes a state of plane-strain stress in any thick connection where ductility is lost and sudden fracture can occur.

Medium joint restraint results in relatively high weld shrinking strains and low global restraint. The welds shrink but the members, effectively pinned on rollers by the erection bolts or other bracing fixtures, are relatively free to move. The strain graphs in Figures 15 and 16 show high strains remaining in Joint 3 welds after welding, while the displacement graphs of the columns in Figures 19 and 20 essentially equilibrate at their original starting points. Importantly, the strain graphs show regions of compression remaining within the medium-restraint connections. The compression is a function of the bending moments building within the connection the structure freely reacts against the increasing weld layers. Compression assures ductility in the Boundary 1, pinned connection. Triaxiality will not occur in a joint under medium restraint.

High joint restraint results in high tensile strains and high global restraint. The strains created by welding the closing seam prestress the welded connections and translate throughout the structural frame. Medium restraint quickly changes to high restraint as the tension in the closing weld overcomes the compression that remained in the previously welded joint. The strain graphs in Figures 14 through 17 showed the resistance of the test fixture to the thermal welding displacement. Joints 2, 4-1, and 4-2 doubled the strain on the frame over that of the medium restraint joint. Triaxial joint restraint, longitudinally along the weld, transversely across the weld, and axially through the section's thickness, is predicted for thick weldments characterized by the Boundary 2, fixed connection experiments.

Under high joint restraint, the columns bend out of their vertical plane after the closing weld is made. The final displacement of LVDT 1 and 6 at the exterior columns shown in Figures 18 through 20 indicate the columns bend toward the weld after welding. While the actual experimental displacements are small, the column is stubby; less than 1.8 m (72 in.) tall. The section's second moment of inertia resisting displacement is very high. The column is fixed, out-of-plane by the closing welds 2, 4-1, and 4-2 while the flange was expanded from preheat and residual welding heat. Depending upon the global structure restraining the connection, greater out-of-plane displacement will be observed in longer, unbraced sections.

The data from LVDT 3 and 4 in Figures 19 and 20 illustrate the trade-off between displacement in the welded joints and the build-up of residual welding stress. Stress increases with decreasing joint displacement regardless of the global restraining conditions. And the overall tension welded into the test fixture frame was confirmed

when WT-3 was cut out of the frame. The displacement data in Table 9 and the strain data in Table 10 derived when removing WT 2 and 3 show between 117.2 MPa (17 ksi) and 172.4 MPa (25 ksi) tensile stress remaining in the test frame after welding the highly restrained joint. The residual welding stress is preloaded into the connection before any service loads are imposed and represented between 34% and 50% of the designed connection yield strength. Without any compensating compressive stress, a field of plane-strain stress develops in the thick connection.

#### 4.2. Welding Displacement and Medium Joint Restraint

Increasing the weld area increased the joint displacement, up to a point. Eventually, the early weld layers locked up all of the joints, regardless of the area. The early layers restrained the joints from inside of the weld. The points where displacement virtually stops and the strain starts climbing in Figure 14 and Figure 15 identify when the medium restraint is first placed on the connection. These data challenge the AWS displacement equations in 1.5.2. The AWS equations do not consider the impact of medium joint restraint on thermal displacement and predict much greater displacement than actually was observed. The variables of both equations center upon joint configuration and do not consider medium joint restraint from welding. The experimental data were seldom closer than 33% of the calculated displacement using Equation 5. Actual displacement was less than half the displacement calculated by the AWS equation used today, Equation 6. Deviation from the calculated displacement increased in the highly-restrained, closing joints. This AWS equation repeatedly predicted displacement more than twice that measured during the experiments.

### 4.3. Weld Tempering

Though joint restraint restricted the theoretical thermal displacement predicted by the displacement equations, the resulting residual welding stresses were never as high as the design yield strength. As noted in 2.1.2, the welding literature frequently repeats the assumption that residual welding stress approaches the yield strength of steel. This assumption was not observed in the present experiments. The welding strains measured while welding the medium-restraint joints were low in comparison with the highly restrained joints. The greatest experimental stress created by medium joint restraint was only 34.5 MPa (5 ksi), 90% lower than the 345 MPa (50 ksi) yield strength expected for A992 steel. The greatest strain recorded after welding highly restrained Joint 4-1 in WT-3 was 174 MPa (25 ksi), again substantially below the steel's yield strength. It appears the repeated heat input from the welding arc tempers thick welds. Figure 2 suggests that the welding heat temporarily reduces the local yield strength to relieve much of the strain in previous weld layers. Tempering does not relieve all of the strain, however. Residual tension hovers in the background of each weld to reduce joint ductility.

### 4.4. Fabrication Sequences

The overall thermal displacement of WT-1 and WT-2 was large compared with WT-3 and WT-4. This difference was due to a change in the assembly sequence of the beam-to-column welds. All of the welds were made in rapid sequence, one right after the other. The welds in WT-3 and WT-4 were permitted to cool and return to their equilibrium positions before the closing welds were made. This change decreased the displacement of the structure by approximately 90% and the strains imposed by almost 18%. General fabrication practice welds all of the truss connections in a bay before

moving on to the next. As shown experimentally, this technique fixes much of the thermal displacement into the connection region. Fabricators and erectors should weld the web members to one chord first, proceeding from the most restrained location to the least. The welded chord should be allowed to cool to equilibrium for at least 4 hours. Finally, the second chord member should be joined to the web members. Welding should proceed from the most restrained connection to the least restrained. This welding plan will reduce the residual welding stress.



## 5. RECOMMENDATIONS FOR FURTHER STUDY

This thesis attempts to characterize medium and high joint restraint, two levels not well documented in today's engineering literature. Literature characterizing the effects of warping, distortion, and other forms of thermal displacement largely describes methods that restrain shifting components (Lincoln 1994). Whether restraining the joint regionally by fixtures and clamps or restraining the joint globally in a stiff assembly, reducing the potential displacement of a weld can only come at some increase in tensile residual welding stress at the expense of the structural design. Restraining techniques may be suitable for relatively thin sections with some available degrees of freedom, but restraint in large, heavy weldments only promotes fracture. Plane-strain stress, induced triaxially by welding, limits the engineer's opportunity to predict when ductile failure will safely occur.

At this time, there is little opportunity to reduce residual stress with the arc welding procedure. The thermal energy needed to melt the filler and base metals falls in a relatively narrow range of amperage, voltage, and speed of travel parameters. Electrodes operate within a narrow range of optimum electrical parameters governed largely by the size and type of electrode. The base metal thickness largely determines the speed of travel needed apply the thermal energy created by welding. If the heat input gets too cold, mechanical welding defects will increase and the metallurgical structure will be inferior. If the heat input is increased, the filler metal does not enter the weld puddle smoothly and the welder soon loses control of the molten metal. While special heat control can improve

the as-cast grain structure, it does little to change the strain and thermal displacement remaining in the weldment. Preheating the base metal has no effect upon thermal displacement unless heat is applied strategically to prebend a member with Region L<sub>2</sub> displacement, out-of-plane. Most preheat operations are performed to control the weld quench rate for improved grain structure, not for strategic prebending.

It is obvious from the differences between WT 1 and 2 and WT 3 and 4 that the structural assembly sequence must be carefully detailed to minimize the resultant strains that remain in the system. Fabricators and erectors can develop weld plans the engineer can review for impact to the structural framework. Traditional assembly sequences will need modification to minimize residual welding stress. The connection nodes along the compression chord should be welded first. All of these welds should be allowed to cool to equilibrium before welding the web members to the opposite chord. This technique would minimize the regional displacement of the connection region created by welding on one chord flange. Minimizing out of plane deviation of the connection would improve the chord's resistance to Euler buckling under load. Erectors might consider preheating the far-side flange of a column before welding. Preheating the flange away from the connecting flange will prebend the connection away from a closing weld. Welding displacement will pull the column into plane and reduce secondary bending effects. Current practice joins the flanges of beam-to-column first and web last. This technique pins the web weld in place before welding and will increase residual welding stress. Welding from the most restrained area in the web out to the least restrained at the flanges permits some thermal displacement through the joint to self-relieve the weld stresses.

A better understanding of Region L<sub>2</sub> thermal displacement is needed. Much of the

## REFERENCES

- AISC. (2005). *Steel construction manual*, 13<sup>th</sup> Edition, American Institute of Steel Construction, Chicago Il., 16.3-27 – 16.3-45.
- ASM. (2002). *Failure analysis and prevention*, *ASM handbook*, Vol. 11, ASM International, Materials Park Oh., 1053.
- ASME. (2001). *2001 ASME boiler & pressure vessel code*, 2003 Addenda, American Society of Mechanical Engineers, New York NY., 648.
- ASTM. (2005). *A6/A6-05 standard specification for general requirements for rolled structural steel bars, plates, shapes, and sheet piling*, ASTM International, West Conshohocken Pa., 17 – 21.
- ASTM. (1972). *STP 503 elevated temperature static properties of wrought carbon steel*, ASTM, Alpha NJ., 25.
- AWS. (2008). *D1.1 structural welding code – steel*, American Welding Society, Miami Fl., 200 – 202.
- Blodgett, O. (1976). *Design of weldments*, The James F. Lincoln Arc Welding Foundation, Cleveland Oh., 6.5-5.
- Blodgett, O. (1998). “The effect of constraint on ductility in welded beam-to-column connections.”, *Proceedings of the 1998 National Steel Construction Conference in New Orleans 4/1-3/98*, American Institute of Steel Construction, Chicago Il., 5 – 3.
- DaDeppo, D. (1999). *Introduction to structural mechanics and analysis*, Prentice Hall, NJ., 103.
- Dexter, R. et al. (2002). “Ductility and strength requirements for base metal in welded T-joints.” *Journal of Materials in Civil Engineering*, 14(1), 38.
- Dieter, G. (1986). *Mechanical metallurgy*, 3<sup>rd</sup> Edition, McGraw Hill, San Francisco Ca., 46.
- Evans, G., and Bailey, N. (1997). *Metallurgy of basic weld metal*, Abington Publishing, Cambridge England, 3 – 4.

FEMA. (2000). "Recommended seismic design criteria for new steel moment-frame construction.", *FEMA 350*, Federal Emergency Management Agency, Washington DC., 1 – 4.

Honeycombe, R., and Bhadeshia, H. (1995). *Steels microstructure and properties*, 2<sup>nd</sup> Edition, Butterworth Heinemann, New York NY., 300.

Lincoln Electric. (1994). *The procedure handbook of arc welding*, 13<sup>th</sup> Edition, Lincoln Electric Company, Cleveland Oh., 3.1-18.

Masubuchi, K. et al. (1987). *Welding handbook, vol. 1*, 8<sup>th</sup> edition, American Welding Society, Miami Fl., 225 – 249.

Schafer, B., et al. (2000). "Triaxiality and fracture of steel moment connections." *Journal of Structural Engineering*, 126 (10), 1131 – 1139.

Vishay Micro-Measurements. (2007). "Strain gage thermal output and gage factor variation with temperature." *Document Number 11054*, revision 15-Aug-07, Malvern Pa., 40 – 41.

Zhang, J. and Dong, P. (2000). "Residual stresses in welded moment frames and implications for structural performance." *Journal of Structural Engineering*, 126 (3), 306 – 315.